"The properties of ferromagnetic materials at high frequencies".

Thesis submitted by J. B. Birks, B.A.(Oxon.), candidate for the degree of Doctor of Philosophy, at the University of Glasgow.

May 1949.

ProQuest LLC.
789 East Eisenhower Parkway
P.O. Box 1346
Ann Arbor, MI 48106 – 1346

Acknowledgements.

The work described in this thesis was undertaken in the Department of Natural Philosophy, Glasgow University, under the supervision of Professor Dee. The author wishes to acknowledge his tenure of an Imperial Chemical Industries Research Fellowship during the initial part of the research (1946-7), and also his indebtedness to the Chief Superintendent, T.R.E. for the loan of certain centimetre wave valves and ancilliary apparatus used in the experiments.

THE PROPERTIES OF FERROMAGNETIC MATERIALS AT HIGH FREQUENCIES

INDEX

THE PROPERTIES OF FERROMAGNETIC MATERIALS AT HIGH FREQUENCIES.

1. INTRODUCTION

1.1. Dielectric and magnetic dispersion.

The dielectric dispersion and absorption of materials at high frequencies have been the subject of extensive study for several decades. The theory of dipole moments and polar relaxation processes (Debye, 1929) has reached a sufficiently advanced stage, that the study of dielectric spectra has become one of the standard methods of investigating structural and molecular properties.

The behaviour of paramagnetic solids in high-frequency fields is similar to that of dielectric materials. The contribution of the magnetic dipoles to the paramagnetic susceptibility decays away by relaxation processes, analogous to those observed in polar dielectrics. The investigation of paramagnetic relaxation and its dependence on temperature and external fields has led to the development of a satisfactory theory of the thermodynamic processes in these materials (Gorter, 1947).

In comparison, the study of the magnetic dispersion and absorption of ferromagnetic materials

at high frequencies is at a much less advanced stage. All the previous experimental work on high-frequency permeability, with the exception of a few isolated measurements, has been concerned with ferromagnetic metals, probably because of their technological interest. Much of the experimental data is conflicting, and due to inherent difficulties of measuring the true high-frequency permeability of conducting materials, it is often presented in a form which is not amenable to direct analysis. Various alternative theories of ferromagnetic dispersion have been proposed, but little success has yet been achieved in correlating these with the experimental observations.

1.2. Previous work on ferromagnetic metals.

At low frequencies the permeability of a ferro:magnetic material may be measured directly, but at high frequencies it can only be derived indirectly from measurements of the electromagnetic properties of a circuit or system containing the material. Ferromagnetic metals, because of their high conductivity, have been studied as conducting elements in high frequency circuits, transmission lines or cavity resonators. Four parameters R, G, L and C, the resistance, conductance, inductance and capacitance per unit length, define the properties of

such systems. Two of these, R and L, are dependent on the permeability of the conductors. Thus in a coaxial line in which the radius, resistivity and permeability of the inner and outer conductors are respectively r_1, ρ_1, μ_1 and r_2, ρ_2, μ_2 at a frequency ν, R and L are given by the classical equations,

$$R = \sqrt{\nu}\left[\frac{\sqrt{\mu_1\rho_1}}{r_1} + \frac{\sqrt{\mu_2\rho_2}}{r_2}\right] \qquad (1)$$

$$L = 2\log\frac{r_2}{r_1} + \frac{1}{2\pi\sqrt{\nu}}\left[\frac{\sqrt{\mu_1\rho_1}}{r_1} + \frac{\sqrt{\mu_2\rho_2}}{r_2}\right] \qquad (2)$$

All the experimental methods, which have been used, fall into one or other of two categories, based on the measurement of either (a) the resistive component R, or quantities related to it, such as the attenuation or Q-factor of the system (Table 1), or (b) the inductive component L or related quantities, such as the wave-velocity or the resonant frequency (Table 2). The permeability μ_R derived from measurements of the resistive losses of the high-frequency circuit, differs from the value μ_L obtained from measurements of the circuit inductance. It has been shewn (Arkadiew, 1913; Kittel, 1946) that this anomaly arises from the implicit assumption that μ is a real (rather than a complex) quantity at high frequencies. By confirming the

Table 1 - Resistive measurements. (μ_R)

Method	Observers
Resistance of wires in resonant circuit, by substitution method.	Webb (1938) Hoag and Cox (1940)
Resistance of heater wire in thermo-junction.	Strutt (1931) Schwarz (1932) Mohring (1939)
Resistance of lecher-wires, by Wheatstone bridge method.	Kreielsheimer (1933)
Resistance of ferromagnetic wire, by lecher-wire impedance bridge method.	King (1935)
Attenuation along lecher-wires by standing-wave method.	Arkadiew (1919) Michels (1931)
Absorption of waves by wire grating.	Arkadiew (1914,24,26)
Q-factor of lecher-wire system, bridged by ferromagnetic wire.	Potapenko and Sanger (1933, 37)
Q-factor of resonant cavity, having one ferromagnetic wall.	Griffiths (1946) Yager and Bozorth (1947)
Q-factor of coaxial resonator, with ferromagnetic inner conductor.	Johnson, Rado and Maloof (1947)
Absorption of waves by ferromagnetic film.	Simon (1946)

Table 2 - Inductive measurements. (μ_L)

Method	Observers
Inductance of lecher-wires, by Wheatstone bridge method	Kreielsheimer (1933)
Inductance of coil with ferromagnetic material, in resonant circuit.	Dannatt (1936) Volkova (1932)
Wavelength on lecher-wire system.	Lindman (1938) Procupiu and d'Albon (1937) Michels (1931) Hoag and Gottlieb (1939) Hoag and Jones (1932)
Wavelength on coaxial line, with ferromagnetic inner conductor.	Glathart (1939) Schmidt (1948)
Resonant length of copper lecher-wire system, bridged by ferromagnetic wire.	Potapenko and Sanger (1933, 37)
Resonant frequency of tuned circuit, containing ferro: :magnetic material.	Wait (1927) Woods (1942)
Resonant frequency of coaxial resonator, with ferromagnetic inner conductor.	Johnson, Rado and Maloof (1947)
Reflection of waves by wire grating	Arkadiew (1914,24,26)

measurements to either the real or imaginary component of the circuit impedance, different values of the apparent real permeability μ_R and μ_L are obtained, neither of which is equal to, or simply related to, the true permeability μ. The equations (1) and (2) on which the measurements are based, are in fact only valid simultaneously when μ is real and $\mu_R = \mu_L$.

The measurement of both impedance components of the same circuit, and the consequent determination of μ is made difficult by the presence of a high conductivity, associated with the permeability. The majority of observers have, therefore, confined themselves to measurements of either μ_R or μ_L. The experimental data on iron, reviewed by Allanson (1945), is shewn in Figure 1. Although the results shew certain general trends, there are obvious major discrepancies to be accounted for. The most consistent data is that in the frequency region above 200 Mc/s.

The macroscopic properties of ferromagnetic materials are normally interpreted in terms of translational and rotational motions of the domains, which form the fundamental structural units and whose

dimensions are of the order of 10^{-3} to 10^{-4} cm. By analogy with the relaxation observed in dielectric and paramagnetic materials, ferromagnetic dispersion associated with the internal restraints on such domain motions might be expected theoretically. Various alternative mechanisms have been proposed to account for the dispersion process along these lines, by considering the restraints due to magnetic viscosity (Arkadiew, 1913), due to eddy-current fields (Becker, 1938) and due to anisotropy forces (Landau and Lifshitz, 1935). These theories will be considered in more detail in § 8.

None of these theories accounts satis: :factorily for the magnetic dispersion in iron and other ferromagnetic metals above 200 Mc/s. The reason for this has been pointed out by Kittel (1946). In metals, the high conductivity restricts the penetration of the high-frequency magnetic field to a thin surface layer. The skin-depth in iron at 200 Mc/s is only about 10^{-4} cm., which is less than the average thickness of a single domain. The dispersion observed at higher frequencies is, therefore, associated primarily with the incomplete penetration of the surface domains. It is not due

to internal domain phenomena, which cannot be observed, because of the intense skin-effect.

1.3. Ferromagnetic materials of low conductivity.

A consideration of this previous work on metals suggested that an investigation of the high-frequency properties of ferromagnetic materials of low conductivity would be of interest. These materials offer several advantages. The experimental difficulties and anomalies experienced with metals, due to their high conductivity, can thereby be avoided. In the wave-impedance methods possible with low-conductivity materials, both the complex permeability and permittivity can be measured, without introducing relations, such as (1) and (2), which are of limited validity. Moreover, since the high-frequency field is able to penetrate much more deeply than in a metal, it is possible to observe internal domain effects, which would otherwise be observed by the skin-effect.

Previous work on the high-frequency permeability of ferromagnetic materials of low conductivity is in general scanty, and of limited interest. Most of the observations have been made at relatively low frequencies below 20 Mc/s, by

introducing specimens into air-cored coils, and determining μ_L from the inductance change, measured by tuned-circuit or impedance-bridge methods. The true permeability cannot be obtained thus, since the dielectric losses prevent the magnetic absorption being measured independently. The method has been used by Foster and Newton (1941) on iron-dust cores of unspecified composition from 1-50 Mc/s, by Wait (1927) on magnetite dust at 3 Mc/s, and by Zimowski (1937) on various ferromagnetic compounds (magnetite, haematite, pyrites etc.) from 5-20 Mc/s. Measurements have also been made up to 1 Mc/s by Snoek and his co-workers at Eindhoven, on the properties of the ferrites (Snoek, 1947a).

The only measurements known at higher frequencies, prior to the present investigation, were those carried out in Germany, during the war, on the "Schornsteinfeger Project". The results obtained in 1945 by Huttig and Flegler on δ-ferric oxide at wavelengths of 174, 77.5 and 39.5 cm. are listed in Table 3. The data is taken from a report (MacFarlane, 1945) based on captured documents. No details of the experimental method used are given. The trend of these observations suggests the occurrence of magnetic dispersion and absorption in

Table 3 - γ -ferric oxide (Huttig)

λ (cm.)	174	77·5	39·5
$\lvert\mu\rvert$	5·9	5·3	4·6
$\tan\delta_\mu$	~ 0·0	0·30	0·46
ϵ	5·23	5·4	5·4

the microwave region. It was, therefore, decided to investigate the properties of low-conductivity ferromagnetic materials at wavelengths from 60 cm. down to 1.25 cm., the limit set by the microwave oscillators available.

2. GENERAL PRINCIPLES OF MEASUREMENT

2.1. Impedance concept.

The permeability μ and the permittivity ϵ of a medium, relative to their free-space values, can be defined in oscillatory fields by Maxwell's electro-magnetic equations for the medium,

$$\text{Curl } E = -\frac{\mu}{c}\frac{\partial H}{\partial t} \qquad (3)$$

$$\text{Curl } H = \frac{\epsilon}{c}\frac{\partial E}{\partial t} \qquad (4)$$

An alternative and equivalent definition, which is more convenient in the present context, is provided by the impedance concept, developed by Schelkunoff (1938). The properties of the medium are expressed in terms of two parameters, the propagation coefficient γ, and the intrinsic impedance z, relative to free space. The propagation coefficient of the medium,

$$\gamma = i\frac{2\pi}{\lambda}(\mu\epsilon)^{\frac{1}{2}} \qquad (5)$$

where λ is the free-space wavelength, determines the phase velocity (imaginary component of γ) and the attenuation constant (real component of γ). The relative intrinsic impedance

$$z = (\mu/\epsilon)^{\frac{1}{2}} \qquad (6)$$

is defined as the ratio of the electric and magnetic fields in a plane wave propagated through the medium, compared with the free-space ratio.

z determines the reflection and transmission coefficients of a wave at a boundary of the medium. Thus at normal incidence, the reflection and transmission coefficients r_{12}, t_{12}, at the boundary of two media, relative intrinsic impedances z_1, z_2, are given by

$$r_{12} = \frac{z_2 - z_1}{z_2 + z_1} \qquad (7)$$

$$t_{12} = \frac{2 z_2}{z_2 + z_1} \qquad (8)$$

In some wave systems it is simpler to treat these coefficients, rather than the intrinsic impedances, as fundamental. A formal theory, based on generalised reflection and transmission coefficients, has been developed by the author (1946a), and applied to multiple dielectric media. For the present purpose, the impedance concept is more suitable.

2.2. Complex permittivity and permeability.

In principle, determinations of μ and ϵ at high frequencies resolve into measurements of z and γ, or quantities equivalent to them in the particular transmission system used. For non-magnetic materials, the permeability $\mu = 1$, and the permittivity ϵ can, therefore, be derived from measurements of either z or γ. ϵ is in general complex and may be written

$$\epsilon = \epsilon' - i\epsilon'' = |\epsilon| e^{-i\delta_\epsilon} \qquad (9)$$

where

$$\tan \delta_\epsilon = \epsilon''/\epsilon' \qquad (10)$$

is called the dielectric loss tangent.

For ferromagnetic materials, a measurement of both the complex quantities z and γ is necessary and sufficient for the determination of μ and ϵ. These properties are then given uniquely, from (5) and (6), by

$$\mu = -\frac{i z \gamma \lambda}{2\pi} \qquad (11)$$

$$\epsilon = -\frac{i \gamma \lambda}{2\pi z} \qquad (12)$$

When measurements of z and γ lead (as do the

observations to be described) to both a complex ϵ and a complex μ, these quantities represent the macroscopic permittivity and permeability of the material, as defined by (3) and (4). A complex permeability may be written

$$\mu = \mu' - i\mu'' = |\mu| e^{-i\delta_\mu} \qquad (13)$$

where

$$\tan \delta_\mu = \mu''/\mu' \qquad (14)$$

is the magnetic loss tangent.

Maxwell's equations, being originally based on the static properties of materials, are commonly formulated in terms of three <u>real</u> parameters, ϵ, μ and σ, the conductivity. Dielectric absorption is then described in terms of an equivalent conductivity, although the absorption may arise from other causes. It is, however, impossible to describe magnetic absorption in terms of three real parameters; a fourth one must be introduced for the purpose. The breakdown of equations (1) and (2) in a region of magnetic absorption occurs, because they are both derived from the classical 3-parameter form of Maxwell's equations.

The adoption of (3) and (4) as

fundamental, without restrictions on the nature of ϵ and μ, avoids this anomaly. Reversing the earlier procedure, conductivity can now be expressed in terms of ϵ''. No static equivalent of μ'' exists, since magnetic absorption is a dynamic effect only.

2.3. Free-space impedance methods.

The intrinsic impedance z of a material can in principle be obtained from the reflection coefficient (7) of a plane wave, incident in free-space, on the boundary of a semi-infinite specimen, i.e. of sufficient thickness that the reflection from the second face is negligible. The relative input field-impedance

$$z_\infty = z \qquad (15)$$

(Field-impedances, like intrinsic impedances, are expressed relative to the intrinsic impedance of free space). In practice, however, unless the material has a very high absorption, one is restricted to measurements on a specimen of finite thickness, d, terminated in a relative field-impedance z_f. The input field-impedance

z_i is then given by

$$z_i = z \frac{z_f + z \tanh \gamma d}{z + z_f \tanh \gamma d} \qquad (16)$$

The simplified forms of (16) obtained for $z_f = 0$, and $z_f = \infty$, form the basis of a method suitable for poorly-conducting ferromagnetic materials. The former case corresponds to the specimen being terminated in a short-circuit, and the relative input impedance is

$$z_{sc} = z \tanh \gamma d \qquad (17)$$

The latter case corresponds to an open-circuit termination, giving

$$z_{oc} = z \coth \gamma d \qquad (18)$$

Combining (17) and (18), solutions are obtained for z and γ in terms of the measurable quantities z_{sc}, z_{oc} and d,

$$z = (z_{sc} z_{oc})^{\frac{1}{2}} \qquad (19)$$

$$\gamma = \frac{1}{d} \operatorname{arc\,tanh} (z_{sc}/z_{oc})^{\frac{1}{2}} \qquad (20)$$

3. THEORY OF WAVEGUIDE IMPEDANCE METHOD

The free-space method, outlined in § 2.3, though feasible, would involve taking measurements on large sheets of the ferromagnetic material. This limitation may be overcome by the use of transmission lines, for which only small specimens are required, and on which measurements can be made with much greater precision. The experimental method which has, therefore, been adopted is the transmission-line analogue of the free-space method. Coaxial lines are used at wavelengths of 60 -6 cm., and H_{10} rectangular waveguides at wavelengths of 3 cm. and 1·25 cm. Both types of transmission line may be referred to as waveguides.

Observations are made on a specimen of the ferromagnetic material, filling a section of length d at the output end of a waveguide. Measurements are made of the amplitude and phase of the voltage standing-wave on the input waveguide when the specimen is terminated (a) by a short-circuiting plate, and (b) by a closed quarter-wavelength section of waveguide, which is equivalent to an open-circuit. From these measurements, the input impedance z'_i, relative to the characteristic impedance of the empty

waveguide, is obtained for the short-circuit and open circuit conditions (= z'_{sc} and z'_{oc} respectively). The relative input impedance is given by

$$z'_i = \frac{1/n - i \tan\beta l}{1 - i(\tan\beta l)/n} \qquad (21)$$

where n is the standing wave ratio (ratio of voltage maximum to minimum), l is the distance of the voltage minimum from the input face of the specimen, β ($= 2\pi/\lambda_g$) is the phase velocity, and λ_g is the measured wavelength on the input waveguide (= λ for the coaxial line).

The relative input impedances z'_{sc} and z'_{oc} are related, by equations similar to (17) and (18), to z' , the characteristic impedance of the filled section, relative to that of the empty waveguide, and γ' the propagation constant of the section. Hence

$$z' = (z'_{sc}\, z'_{oc})^{\frac{1}{2}} \qquad (19a)$$

$$\gamma' = \frac{1}{d} \operatorname{arc\,tanh} (z'_{sc}/z'_{oc})^{\frac{1}{2}} \qquad (20a)$$

For a coaxial line operating in its principal mode, the wave is purely transverse and

$$z' = z = (\mu/\epsilon)^{\frac{1}{2}} \qquad (6a)$$

$$\gamma' = \gamma = i\frac{2\pi}{\lambda}(\mu\epsilon)^{\frac{1}{2}} \qquad (5a)$$

so that (11) and (12) remain valid in the form

$$\mu = -i\,\frac{z'\gamma'\lambda}{2\pi} \qquad (11a)$$

$$\epsilon = -i\,\frac{\gamma'\lambda}{2\pi z'} \qquad (12a)$$

For an H_{10} rectangular waveguide, z' and γ' are also dependent on the cut-off wavelength of the empty guide, λ_c ($= 2a$, where a is the guide width) and are given by

$$z' = \mu\left[\frac{1-(\lambda/\lambda_c)^2}{\mu\epsilon-(\lambda/\lambda_c)^2}\right]^{\frac{1}{2}} \qquad (22)$$

$$\gamma' = i\,\frac{2\pi}{\lambda}\left[\mu\epsilon-(\lambda/\lambda_c)^2\right]^{\frac{1}{2}} \qquad (23)$$

leading to

$$\mu = -\frac{iz'\gamma'\lambda_g}{2\pi} \qquad (24)$$

$$\epsilon = -\frac{i\gamma'\lambda^2}{2\pi z'\lambda_g}\left[1-\left(\frac{\pi}{\gamma' a}\right)^2\right] \qquad (25)$$

where λ_g is the wavelength in the empty guide. Thus in both types of transmission line, μ and ϵ are obtained in terms of measurable quantities.

4. DESCRIPTION OF APPARATUS

4.1. Waveguide and detector systems.

The input voltage standing-wave is measured by means of a tuned crystal detector, mounted in a sliding carriage, which is moved manually along the length of the waveguide. A short thin probe from the detector projects into the waveguide through a narrow longitudinal slot, milled parallel to the axis of the guide and, in the case of the H_{10} rectangular waveguide, along the centre of its broad side. The high frequency voltage induced in the probe is rectified by the crystal, and the crystal current is measured by a sensitive galvanometer. The tuning of the detector by means of a variable reactance stub increases its sensitivity and discriminates against the detection of harmonics. Particular care has been taken in the mechanical construction to ensure that the probe moves centrally along the guide, and that its depth of penetration remains constant as the position of the carriage is varied.

The general arrangement of the complete apparatus used on each of the four wavelength ranges (60 - 20 cm., 15 - 6 cm., 3 cm. and 1·25 cm.)

is similar, and it differs only in detail from the schematic diagram (Figure 2).

4.2 60 - 20 cm. apparatus.

For measurements at wavelengths from 60 cm. to 20 cm. a variable frequency triode oscillator (446 tube with concentric line tuning) is used. The oscillator output, which is monitored by a bolometer bridge circuit, is loosely coupled through a concentric cable to the slotted coaxial waveguide. The coaxial has an outer conductor diameter of 4.45 cm., an inner conductor diameter of 1.35 cm. and a slot length of 110 cm. The inner conductor which is constructed of light thin-walled tube to give rigidity is supported at intervals by sets of three thin polystyrene rods, screwed through the outer conductor, at 120° to each other. These spacing rods have been found to have little effect on the phase velocity in the line, but to avoid any such errors being introduced into the standing-wave measurements, no spacers are used in the last 50 cm. of the line. The inner conductor is supported at the output end by the specimen and termination. The position of the detector carriage is measured by a 0·01 cm. vernier scale.

4.3. 15-6 cm. apparatus.

At wavelengths near 9 cm., a standard reflex klystron oscillator (CV67) is used. For other wavelengths in this range, a modified klystron oscillator has been constructed (Figure 3). The central rhumbatron cavity of the oscillator is extended on each side by rectangular waveguide sections, whose length may be varied by short-circuiting pistons, geared to move in synchronism. By adjustment of the electrode voltages, and thus modifying the transit-time of the velocity-modulated electron beam through the drift-space between the cavity gap and the reflector, high-order modes of oscillation of various wavelengths from 16 cm. to 5 cm. can be induced in this composite cavity. Care is exercised in the choice of suitable modes, to ensure that the oscillations are stable and monochromatic.

The klystron oscillator is loosely coupled to a long length of cable, feeding the coaxial. The coaxial line has an outer conductor diameter of 2·225 cm., inner conductor 0·775 cm., and a slot length of 16 cm. The inner conductor is supported at the input end by

a polythene insulator, and at the load end by the sample and termination.

The position of the detector carriage is measured by two 1" micrometer dial gauges (calibrated in 0·001" divisions) which are mounted on the coaxial line, on opposite sides of the carriage, and bearing against it. The gauges are positioned to record consecutive 1" traverses of the carriage along the line. For the longer wavelengths, where a greater movement is necessary for the standing-wave measurements, a single dial-gauge is used, and calibrated 1" and 2" sliding steel blocks are placed between the detector carriage and the dial-gauge probe to extend its range.

4.4 3 cm. and 1·25 cm. apparatus.

At wavelengths near 3 cm., a CV 129 reflex klystron oscillator is used. The oscillator is coupled to a short coaxial cable, which terminates in a probe feeding the 1" x $\frac{1}{2}$". H_{10} rectangular waveguide system. A fraction of the input power is tapped off, through a gap in the short-circuiting plate behind the probe, to a fixed crystal detector, which monitors the

power fed to the waveguide system. The fixed attenuator, which consists of a flat prism of lossy dielectric material, attached to the broad inner face of the waveguide, has an attenuation of about 6 decibels, and serves to minimise frequency-pulling due to changes in the load impedance. The variable attenuator consists of a thin circular segment of resistive material (carbonised bakelite), which may be lowered into the guide through a longitudinal central slot in the broad face of the guide. By this means, up to 40 db. of attenuation may be introduced, without mismatching the oscillator. The attenuator is used for setting the detector crystal current at the level required. (At longer wavelengths this is done by varying the depth of penetration of the probe). The slotted waveguide section has been machined from brass plate to obtain the required constructional accuracy, the internal cross-sectional dimensions being constant to 0·1%. The position of the crystal detector is measured by a micrometer dial gauge, attached to the detector carriage, and bearing against a fixed block on the side of the waveguide.

The apparatus used at 1·25 cm. wavelength is similar, except in minor details. The reflex klystron oscillator (an experimental type, developed by E.M.I.) feeds directly into a 0·42" x 0·17" H_{10} rectangular waveguide system. The power is monitored by a fixed crystal detector situated between the fixed and variable attenuators. The position of the detector carriage, which is moved along the slotted guide by a simple frictional drive mechanism, is measured by a micrometer dial-gauge fixed relative to the guide, and bearing against the end of the carriage.

5. EXPERIMENTAL PROCEDURE

5.1. Crystal calibration.

An initial investigation was made of the high-frequency rectifying characteristics of the crystals used. Measurements were made at 9 cm. wavelength, with the slotted coaxial line empty and short-circuited. The crystals were inserted in turn into the detector, and the crystal current I measured as a function of x, the distance along the line of the detector from the current minimum. Since the voltage distribution on a lossless short-circuited line is sinusoidal, the high-frequency voltage V is proportional to $\sin\beta x$. The results may be summarised as follows. The crystals have a square-law characteristic (I proportional to V^2) for crystal currents up to a few microamperes. At higher currents, they deviate in different degrees, often considerably, from the square law. Mechanical shock and ageing may affect the sensitivity and the characteristic, but they do not appear to alter the square-law property at low currents. The characteristic is markedly dependent on the galvanometer circuit resistance, the optimum resistance for $I \propto V^2$ over the widest range, being of the order of 400 ohms. (Figure 4).

It was, therefore, decided to make all standing-wave measurements at low crystal currents, using a spot galvanometer with a sensitivity of 1 μa. for full-scale deflection, and an internal resistance of 400 ohms. The alternative superheterodyne method of mixing the detector current with a large signal from a second high-frequency oscillator and amplifying the resultant intermediate-frequency signal, (Collie, Ritson and Hasted 1946) would involve the duplication of each of the oscillators, and it was not, therefore, considered practicable.

An overall check on the performance of each of the waveguide systems has been made, by measuring I vs. $\sin^2\beta x$ for the empty short-circuited guide as described above, with a maximum crystal current of 1 μa. The constancy of the ratio $I / \sin^2\beta x$ depends not only on the validity of the crystal square law, but also on the accuracy of construction and measurement. Deviations in this ratio may arise from

(a) variations in the depth of penetration of the detector probe,

(b) irregularities in the movement of the carriage,

(c) rectification of any harmonics present,

(d) interaction of the detector probe on the wave in the guide, and

(e) errors in the measurement of current or position.

The results indicate that none of these effects are pronounced, since over the range of currents used in the standing-wave measurements (0·05 to 1 μa.) the variations of $I / \sin^2 \beta x$ are random, for each of the four waveguide systems, and have the maximum values given in Table 4.

5.2. Standing-wave measurements.

The values of the voltage standing-wave ratio n to be measured are often as high as 100 or more. Direct measurement of such large values of n would involve the observation of crystal currents of the order of 10^{-4} μa., if $I_{max} \not> 1 \mu a.$. Apart from observational errors, deviations in the crystal law are likely to become pronounced over so wide a range. Hence, for $n > 3$, an indirect method of determining n from the width of the stationary wave pattern near the minimum is used, which avoids the measurement of either very large or very small crystal currents.

The voltage distribution on a lossless line may be written

$$V^2 = V^2_{min} \left(\cos^2 \beta x + n^2 \sin^2 \beta x \right) \qquad (26)$$

where V_{min} is the minimum voltage, and V is the voltage at a distance x from the minimum. Rewriting

Table 4 - Calibration of apparatus.

wavelength	60 cm.	25 cm.	15 cm.	9 cm.	6 cm.	3 cm.	$1\frac{1}{4}$ cm.
Variation of $I/\sin^2 \beta x$	$\pm \frac{1}{2}\%$	$\pm \frac{3}{4}\%$	$\pm \frac{1}{2}\%$	$\pm \frac{3}{4}\%$	$\pm 1\%$	$\pm 1\frac{1}{2}\%$	$\pm 3\%$

(26) as

$$n^2 = 1 + \left(V^2/V^2_{min} - 1\right) \operatorname{cosec}^2 \beta x \qquad (27)$$

$$= 1 + \left(I/I_{min} - 1\right) \operatorname{cosec}^2 \beta x \qquad (28)$$

for $I \propto V^2$, it is seen that n may be determined from a measurement of x , for a given value of I / I_{min} . For $I/I_{min} = 2$, the standard ratio adopted,

$$n^2 = 1 + \operatorname{cosec}^2 \beta x_0 \qquad (29)$$

where $2x_0$ is the measured distance between points on each side of the minimum at which the crystal current is twice the minimum value (Fig. 5(b)). In a few cases, where $2x_0$ is too small to be measured with reasonable accuracy, I/I_{min} ratios greater than 2 have been used. Since measurements are taken only in the region of the voltage minimum, where the impedance of the guide is low, the probe depth may be made quite large without the introduction of appreciable loss due to the shunt conductance of the detector system. Thus, a much higher sensitivity is obtainable, than in a direct measurement of n .

The distance l from the voltage minimum to the input face of the specimen is measured in

the following manner. The dial gauge or scale, which records the position of the crystal detector, has an arbitrary zero, which must be calibrated. This is done by the measurement of the position b of a voltage minimum, with the guide empty and terminated in a short-circuit (Figure 5 (a)). This minimum is known theoretically to be $m\lambda_g/2$ from the end of the guide (where m is a positive integer). The sample, length d, is then introduced into the guide, and the position c of the voltage minimum is measured (Figure 5 (b)). Equating the distances from the zero of the scale to the end of the guide in each case, we have

$$b + m\lambda_g/2 = c + l + d \qquad (30)$$

and hence

$$\tan\beta l = \tan\beta(b-c-d) \qquad (31)$$

which is the quantity required for substitution in (21). The value of $\lambda_g/2$ and hence β, is obtained from the difference between two consecutive values of b or c.

5.3. Computation

The complete sequence of observations and computation involved in each measurement, may best be illustrated by a typical set of results.

All lengths are in tenths of an inch.

Observations

$d = 1{\cdot}940$

$b = 8{\cdot}059$

and $-3{\cdot}652$ $\therefore \lambda_g = 23{\cdot}422$

	S.C termination	O.C termination		
c =	$4{\cdot}279$	$6{\cdot}252$		
$2x_0$ =	$4{\cdot}246$	$1{\cdot}194$		
$b-c-d$ =	$1{\cdot}840$	$-0{\cdot}133$		
$\tan\beta l$ =	$0{\cdot}5362$	$-0{\cdot}0356$	From	(31)
$1/n$ =	$0{\cdot}4745$	$0{\cdot}1570$		(29)
z'_{sc} =	$0{\cdot}6933 \exp(-i\,34{\cdot}25^\circ)$	$z'_{oc} = 0{\cdot}1610 \exp(i\,12{\cdot}45^\circ)$		(21)
z' =	$0{\cdot}5341 \exp(-i\,10{\cdot}9^\circ)$			(19a)
$\tanh\gamma' d$ =	$2{\cdot}075 \exp(-i\,23{\cdot}35^\circ)$			(20a)
$\gamma' d$ =	$1{\cdot}86 \exp(i\,75{\cdot}95^\circ)$			Chart
γ' =	$0{\cdot}959 \exp(i\,75{\cdot}95^\circ)$			

Results

$\mu = 1{\cdot}20 \exp(-i\,25^\circ)$ (11a)

$\epsilon = 10{\cdot}7 \exp(-i\,3{\cdot}2^\circ)$ (12a)

$\delta'd$ is obtained from the complex hyperbolic tangent, using the Chart Atlas compiled by Kennelly (1914). $\delta'd$ is generally sufficiently small that the principal solution is the valid one, but any ambiguity in the value of $\delta'd$ is resolved by the measurement of a second sample of different thickness.

5.4. Preparation of specimens.

The ferromagnetic compounds which have been investigated are normally obtained in the form of finely-divided powders. Preliminary measurements on specimens formed by simple compression of these powders gave inconsistent results. These are attributable to porosity, the densities of the samples varying between 0·5 and 0.7 of the solid density. Denser materials can be formed by sintering the powders at high temperatures (Snoek 1947a), but apart from the subsequent difficulties of machining these to the required specimen size, the ferromagnetic properties are generally modified by the heat treatment. One of the compounds, γ -ferric oxide, loses its ferromagnetism permanently if heated above 300°C, since it changes into the α -form, which has a different crystal structure and is paramagnetic (Welo and Baudisch 1925).

It was, therefore, decided to mix the powdered compounds with a lossless, non-magnetic base material to form solid samples for measure: :ment. Paraffin wax has been found very suitable for this purpose, because of its low melting point, its negligible dielectric loss, and its plasticity. Mixtures of reasonable homogeneity can be formed by vigorously stirring the compound into molten paraffin wax as it is cooling. The solid mixture is moulded into the required sample shape at room temperature, using a hand-vice for applying pressure. The absence of air-inclusions in the moulded sample is tested by comparing its measured density, with that calculated from the known composition of the mixture. Uniformity of thickness is obtained by turning the sample between the jaws of a steel micrometer, set to the required thickness. The cross-section of the moulded specimen is made slightly oversize, as the material is sufficiently soft to be force-fitted into the waveguide or coaxial line, thereby eliminating experimental errors due to gaps between the sample and the transmission line conductors.

6. MEASUREMENTS ON A γ-FERRIC OXIDE MIXTURE.

6.1. Magnetic dispersion and absorption.

A typical series of observations on a single mixture will be described initially to illustrate the general nature of the results. The mixture contained 32.6% by volume of γ-ferric oxide in paraffin wax.

The magnetic and dielectric properties were measured at 9 different wavelengths ; 58·5, 39·2, 29·8, 22·4, 15·3, 8·93, 5·97, 3·09 and 1·23 cm. Measurements were made at each wavelength on 3 or more specimens moulded from the same material. The mean values of the components of the permeability μ , and of the permittivity ϵ are plotted in Figures 6 and 7. The permeability μ was found to be independent of the strength of the applied field, within the range employed, by repeating observations at different high-frequency field strengths. The initial static permeability μ_s was measured by a ballistic method, and found to be 3·2.

Although the magnetic properties are of primary interest, the simultaneous derivation of ϵ from the same set of observational data provides

an inherent check on the validity of the measure: :ments. The gradual, steady decrease of permittivity with wavelength which is observed (Figure 7) is typical of the dielectric dispersion of solid inorganic compounds. Unusual features in the magnetic dispersion cannot, therefore, be attributed to experimental error. (This point is emphasised, because certain abnormal magnetic dispersion phenomena reported in metals (Kartschagin (1922), Gans and Loyarte (1921), Israel (1926)) were later shown to arise from errors of observation (Wait (1927)).

The accuracy of the observations has been assessed as follows. In the experiments to be described in § 6.2., μ' and μ'' were reduced by 60% and 95% respectively by the application of a large steady magnetic field. The measured value of ϵ, which should be unchanged, was found to remain constant to $\pm 1\%$ for sequences of 10 or more measurements on the same sample. It is considered from such observations that the accuracy of individual measurements, except at the two shorter wave:

:lengths, is of this order. The overall accuracy is, however, limited by local inhomogeneities in the mixture used, which lead to greater variations than this being found between different specimens of the same mixture. Taking this factor into account, it is estimated that the mean values are correct to $\pm$ 2% at wavelengths from 58·5 cm. to 5·97 cm., $\pm$ 4% at 3·09 cm., and $\pm$10% at 1·23 cm.

The magnetic dispersion and absorption (Figure 6) displays several interesting features. From the trend of the observations, it is estimated that the limiting value, μ_0, of μ' on the low-frequency side of the dispersion region ($\lambda \sim$ 150 cm.) is 3·05. Since μ_0 is within 5% of μ_s, the static permeability, (= 3·2) no appreciable dispersion can occur in the interval from $\lambda = \infty$ to $\lambda \sim$ 150 cm. At this latter wavelength μ' begins to decrease, becoming unity at λ = 7·5 cm. while $\tan\delta_\mu$ rises to a maximum at about the

same wavelength. At shorter wavelengths, $\tan\delta_\mu$ decreases again rapidly, and μ' falls below unity, corresponding to a negative susceptibility. At the shortest wavelength of measurement, $\lambda = 1{\cdot}23$ cm., the magnetic loss is negligible, while μ' is approximately unity, which is the ultimate high-frequency value for ferromagnetic materials, indicated by the infra-red measurements of Hagen and **Rubens** (1903). Thus, practically all the magnetic dispersion and absorption of the material occurs in the wavelength interval 150 cm. to 1 cm.

6.2. Effect of magnetostatic field.

Further measurements have been made on the 32·6% γ-ferric oxide mixture to determine the effect of a static magnetic field on the observed dispersion. The moulded specimens were located in the usual manner at the end of the coaxial line, which was placed between the poles of an electro: :magnet, producing a parallel field H normal to the axis. Specimens of similar dimensional ratios were used to avoid

differences in demagnetisation coefficients. The effective values of μ as a function of H were measured at wavelengths from 58·5 cm. to 5·97 cm. The permittivity ϵ was unaffected by H (§ 6.1).

The static magnetisation of the mixture has also been investigated by a ballistic method, and the incremental static permeability μ_s ($= dB/dH$) and its reversible component μ_{sr} have been derived as functions of the applied field H. The results of the static and high-frequency measurements are plotted together in Figure 8. The scale of the static measurements has been adjusted to allow for the demagnetisation coefficients of the coaxial specimens.

The high-frequency and static observations are comparable, since in both cases they represent the effect of a weak field applied to the ferromagnetic material, when it is in the magnetic state produced by a field H. The magnetic dispersion and absorption curves, corresponding to different values of H, are plotted in Figure 9. For

comparison the ordinates are expressed relative to the corresponding values of $\mu_{sR} - 1$. It will be observed that the dispersion retains a similar form, but shifts to shorter wavelengths, and becomes steeper, as the field H is increased.

7. MAGNETIC DISPERSION OF FERROMAGNETIC COMPOUNDS.

7.1. δ -ferric oxide : Effect of concentration.

Measurements have been made on mixtures containing various concentrations of δ -ferric oxide in paraffin wax. The permeability and permittivity curves for the different mixtures are similar to those already described in § 6.1. An attempt has, therefore, been made to extrapolate the observations on the mixtures to zero dilution, and thus derive the properties of the solid material. The initial measurements (1946b), over a limited range of wavelengths and concentrations, agreed reasonably with the classical Clausius-Mosotti relation

$$\frac{\mu - 1}{\mu + 2} = v \frac{\mu_a - 1}{\mu_a + 2} \qquad (32)$$

where μ is the permeability of a mixture containing a proportion v by volume of the oxide, and μ_a is the (extrapolated) permeability of the oxide. Further measurements showed, however, that (32) is of very limited validity, and the alternative

"mixture" laws, reviewed by Guillien (1941) were compared with the observations.

Lichtenecker (1918) proposed, on semi-theoretical grounds, a logarithmic law for the permittivity ϵ of a random dielectric mixture, of the form

$$\log \epsilon = \Sigma \, v \log \epsilon_v \qquad (33)$$

where v is the proportion by volume of the constituent, permittivity ϵ_v, and $\Sigma v = 1$. Applying (33) and its magnetic analogue to the complex permittivity andpermeability, of the oxide-wax mixture, we obtain for the real parts

$$\log |\epsilon| = v \log |\epsilon_a| + (1-v) \log |\epsilon_w| \qquad (34)$$

$$\log |\mu| = v \log |\mu_a| \qquad (35)$$

and for the imaginary parts,

$$\delta_\epsilon = v \delta_{\epsilon_a} \qquad (36)$$

$$\delta_\mu = v \delta_{\mu_a} \qquad (37)$$

where suffix "a" refers to the (extrapolated) properties of the ferromagnetic solid, and suffix "w" to the properties of the wax.

($|\epsilon_w| = 2.28$, $|\mu_w| = 1.00$, $\delta_{\epsilon_w} = \delta_{\mu_w} = 0$)

It is found that, within the experimental error, $|\mu|$ and $|\epsilon|$ for the γ-ferric oxide - wax mixtures vary with v, according to (35) and (34). The experimental values of $|\mu|$ at different wavelengths are plotted on a logarithmic scale against v in Figure 10. The measurements on γ-ferric oxide have been limited to values of v up to 0·41, but Legg and Given (1940), using compressed powdered Permalloy, found (35) to be valid for v up to 1·0, and Buchner (1939) and Wul (1946), using rutile mixtures, found (34) to be also tenable up to 100% concentration.

The magnetic loss angle δ_μ does not increase as rapidly with v, as is indicated by (37). Within the range of the measurements, these observations are more satisfactorily represented by the relation

$$\tan\delta_\mu = v \tan\delta_{\mu a} \qquad (38)$$

The experimental values of $\tan\delta_\mu$ vs v for different wavelengths are plotted in Figure 11. The dielectric loss angle δ_ϵ is sufficiently small, that $\tan\delta_\epsilon \sim \delta_\epsilon$, and (36) or the dielectric analogue of (38) are equally valid.

The values of μ_a and ϵ_a derived from the observations, using (34), (35), (36) and

(38) are given in Table 5. The initial static permeability μ_{as}, extrapolated from measurements on the mixtures in static fields, and the limiting permeability μ_{ao}, at frequencies below the dispersion region, (cf. § 6.1.) have also been obtained. The derived magnetic dispersion and absorption curves for solid γ-ferric oxide are plotted in Figure 12.

The lower values of permeability and permittivity obtainedby Hüttig (Table 3) are attributable to porosity in the compressed samples of oxide which he used. Comparison of his value of $|\epsilon| = 5{\cdot}4$ at $\lambda = 39{\cdot}5$ cm., with the value of $|\epsilon_a| = 84$ from Table 5, leads to $v = 0{\cdot}53$, from (34). This concentration corresponds to that for closest packing of equal spheres in a cubic lattice ($= \pi/6$) Using this derived value of v, Hüttig's measurements of μ and ϵ have been extrapolated to 100% concentration (Table 6). The consistency of these values with those in Table 5 provides a useful check on the extrapolation method.

Table 5 - Solid γ-ferric oxide.

λ (cm.)	$\lvert\mu_a\rvert$	δ_{μ_a}	$\lvert\epsilon_a\rvert$	δ_{ϵ_a}
58·5	21·2	36°	23·9	8·3°
39·2	18·1	45°	24·0	8·8°
29·8	16·9	51°	22·5	8·1°
22·5	12·4	57°	21·7	8·5°
15·3	8·0	61°	20·6	7·2°
8·93	3·2	67°	19·5	6°
5·97	1·4	65°	17·6	5°
3·09	0·53	32°	16·1	4°
1·23	1·2	~ 5°	16	~ 5°

$\mu_{as} = 34$

$\mu_{ao} = 30$

Table 6 - Solid γ-ferric oxide (derived from Table 5)

λ (cm.)	$\lvert\mu_a\rvert$	δ_{μ_a}	$\lvert\epsilon_a\rvert$
174	28·6	~ 0°	22·8
77·5	23·4	29·5°	24
39·5	17·9	41°	24

7.2. Other ferromagnetic compounds.

A similar series of measurements have been made on mixtures containing various concentrations of ferroso-ferric oxide (magnetite) in wax, up to $v = 0{\cdot}55$. The observations of $|\mu|$ and $\tan\delta_\mu$ against v for the different wavelengths of measurement are plotted in Figures 13 and 14. The mixture relations (34) (35) (36) and (38) are again found to be valid, and the properties of the solid material have been similarly obtained by extrapolation. The derived magnetic dispersion and absorption curves for magnetite are plotted in Figure 15.

Similar measurements have been made on mixtures containing manganese-zinc ferrite and nickel-zinc ferrite. These materials, known as "Ferrox-cube 3" and "4", are mixtures of $MnO.Fe_2O_3$ and $ZnO.Fe_2O_3$ and of $NiO.Fe_2O_3$ and $ZnO.Fe_2O_3$ respectively. Their preparation, structure, and general properties have been describedby Snoek (1947a), to whom the author is indebted for supplying powdered specimens. The extrapolated

observations on manganese-zinc ferrite and on nickel-zinc ferrite are plotted in Figures 16 and 17.

The values of μ_o and μ_s for the four compounds (the suffix a will be omitted in the subsequent discussion), obtained from the magnetic dispersion curves, and from static measurements on mixtures respectively, are listed in Table 7.

Table 7 - Comparison of μ_s and μ_o.

Material	μ_s	μ_o
γ -ferric oxide	54	30
Magnetite	15	8
Mn - Zn ferrite	48	44
Ni - Zn ferrite	40	34

8. THEORY OF MAGNETIC DISPERSION

8.1. Nature of Magnetisation Process.

There is a major difference between the microwave magnetic dispersion that occursin metals, and that which is observed in the ferromagnetic compounds. The former is directly associated with skin-effect, and the incomplete penetration of surface-domains (§ 1.2). The magnetic dispersion of the compounds on the other hand, can only be due to an internal magnetisation process, since skin-effect is negligible because of their low conductivity.

The domain theory of ferromagnetism (Becker and Doring, 1939) differentiates four elementary processes which occur in the static magnetisation of a demagnetised material;

(i) Reversible displacements of the Bloch walls, separating adjacent domains.

(ii) Irreversible displacements of the domain walls.

(iii) Irreversible rotations of the spins within a domain from one direction of easy magnetisation to another.

(iv) Reversible rotations of the domain spins, towards the direction of the applied field.

The reversible translational magnetisation (i) takes place in weak fields only, and is generally considered responsible for the initial permeability. The irreversible magnetisation processes (ii) and (iii), which are responsible for the Barkhausen effect, occur in medium fields over the steep portion of the B-H curve. The irreversible component produces the peak in the static μ_s vs H curve (Figure 8). The reversible rotational magnetisation (iv) can occur at all field-strengths, and is theonly process operative in high fields.

Becker (1938) has developed a theory of magnetic dispersion for the translational and irreversible magnetisation components. The dispersion is attributed to the damping action of eddy current fields, induced in the vicinity of domains by the extension of their boundaries, or by irreversible rotations. According to Becker, the irreversible magnetisation component should disappear at relatively low frequencies. The experimental results (Figure 8) confirm this, since the peak in the μ vs H curve has completely disappeared at the lowest frequency used. Hence, only reversible magnetisation processes are operative in the microwave region.

For the relaxation of the reversible domain-wall displacements, Becker obtains a Debye-type equation of the form

$$\frac{\mu - 1}{\mu_s - 1} = \frac{1}{1 - i\nu/\nu'} \qquad (39)$$

for the permeability μ in weak fields of frequency ν , where ν' is the relaxation frequency. The form of (39) is identical with that proposed earlier by Arkadiew (1913), from his theory of magnetic viscosity. This theory was based on Weber's conception of a ferromagnetic material, formed of quasi-independent elementary magnets, and was developed by direct analogy with dipole relaxation in dielectric materials. Becker's eddy-current theory is more in accord with modern interpretations of magnetic phenomena.

Comparison of the observed magnetic dispersion and absorption with (39) reveals several major differences, (e.g. Figure 6). The μ' vs λ curve is steeper than that given by (39) ; the absorption is sharper than the

theoretical one ; and $\mu'-1$ becomes negative, while (39) gives positive values only. The permeability does not, therefore, decay by a relaxation process, as would be expected if it were due to translational magnetisation.

The observations on the effect of an applied field (Figure 9) show that a similar dispersion mechanism operates when high static fields are applied to the material. Translational magnetisation, which can only occur in weak fields, cannot, therefore, be responsible. It is concluded that the magnetic dispersion must be accounted for in terms of the only alternative process, reversible rotational magnetisation, which is operative at all field strengths.

Comparison of the values of μ_o with μ_s (Table 7) shews that, with the exception of magnetite, practically all the magnetic dispersion occurs in the microwave region. If this dispersion is attributed to rotational magnetisation, it follows that the translational magnetisation in these materials is relatively small. This is probably due to the low conductivity, which will inhibit the spread of

eddy currents associated with domain-boundary displacements. Magnetite has a higher conductivity than the other materials investigated, andit appears that the rotational and translational components are of equal magnitudes. ($\mu_s \sim 2\mu_o$). The magnetic dispersion observed in magnetite by Zimowski (1937) at 5-20 Mc/s, probably corresponds to the relaxation of the translational magnetisation. Snoek (1947a) has observed similar low-frequency magnetic dispersion, below 1 Mc/s, in the ferrites.

8.2. Natural ferromagnetic resonance.

The rotation of the spins within a domain towards the direction of the applied field is opposed by the crystalline anisotropy forces, which tend to keep the spins aligned along an easy magnetisation axis On. Landau and Lifshitz (1935) have considered a theoretical domain model of a uniaxial ferromagnetic crystal, and they have suggested that these anisotropy forces are equivalent to an internal magnetic field H_n, acting along On. This natural anisotropy

field, which is of the order of 1000 gauss, arises from spin-orbit interaction, and is distinct from the much larger Weiss molecular field, arising from the spin exchange forces. Landau and Lifshitz have considered the effect of a weak high-frequency magnetic field applied transverse to On, i.e. in such a direction that spin rotation is the only magnetisation process possible. They find that magnetic dispersion takes place as a resonance process, resonance occurring at the Larmor precession frequency ν_n of the electron spins in the internal field, given by

$$h\nu_n = g\mu_B H_n \qquad (40)$$

where g is the Landé factor (= 2 for electron spins) h is Planck's constant, μ_B is the Bohr magneton.

The differences, noted in § 8.1., between the observed magnetic dispersion and absorption and the relaxation equation (39), and, in particular, the negative values of $\mu' - 1$, are characteristic of a resonance process. These observations provide the first

direct experimental evidence of the existence of the internal anisotropy field H_n, predicted by Landau and Lifshitz. As the magnetic properties are due to electronic spin-moments, any magnetic resonance process observed in the microwave region must be due to the presence of a field of the order of 1000 gauss, since for an electron-spin, the Larmor relation (40) becomes numerically

$$H_n \lambda_n = 10.7 \times 10^3 \text{ gauss-cm.} \qquad (47)$$

where $\lambda_n (= c/\nu_n)$ is the resonant wavelength. Since resonance occurs when no such field is applied externally, an effective field H_n must exist within the ferromagnetic material. When an external field H is appliedto the material, it will increase the total field acting on the spins, and the resonance will shift to higher frequencies, as observed (Figure 9). Thus, qualitatively, the observations are consistent with Landau and Lifshitz' theory.

8.3. Induced magnetic resonance.

The conditions within a single domain or region of the polycrystalline material, in which an internal unidirectional anisotropy field H_n exists, will be similar to those in a saturated paramagnetic or ferromagnetic material, in which the spins are aligned by an external polarising field H_n. In the latter case, when an oscillatory field, frequency ν, is applied transverse to H_n, it has been found experimentally that the high-frequency magnetic absorption becomes a maximum at the Larmor frequency of the electron spins in the external static field. This induced magnetic resonance effect is thus closely related to the natural magnetic resonance, due to the internal anisotropy field.

, Induced magnetic resonance has been observed in paramagnetic salts by Zavoisky (1946), Cummerow and Halliday (1946) and others, and in ferromagnetic materials by Griffiths (1946), Yager and Bozorth (1947) and Hewitt (1948). The theory

of the effect has been considered by Frenkel (1945) and Kittel (1947, 48). Frenkel has derived an expression for the high-frequency susceptibility χ of the magnetic material, relative to its static rotational susceptibility χ_0 in a similar transverse field,

$$\frac{\chi}{\chi_0} = \frac{\mu - 1}{\mu_0 - 1} = \frac{\nu_h^2}{\nu_h^2 - \nu^2 + 2i\nu\nu'} \qquad (42)$$

where ν_h is the resonant frequency in the applied field H_h, and ν' is the damping frequency, due to spin-lattice interaction. (The suffix ϕ is used as in § 7 to distinguish the static transverse magnetisation component (i.e. that due to reversible spin rotations) from the total static magnetisation denoted by the suffix s). This expression has been verified experimentally for a saturated ferromagnetic by Yager and Bozorth (1947). The real and imaginary components of susceptibility and permeability are given by

$$\frac{\chi'}{\chi_\phi} = \frac{\mu' - 1}{\mu_0 - 1} = \frac{\nu_h^2 (\nu_h^2 - \nu^2)}{(\nu_h^2 - \nu^2)^2 + 4\nu^2\nu'^2} \qquad (43)$$

$$\frac{\chi''}{\chi_\phi} = \frac{\mu''}{\mu_0 - 1} = \frac{2\nu\nu'}{(\nu_h^2 - \nu^2)^2 + 4\nu^2\nu'^2} \qquad (44)$$

The induced resonance experiments on ferromagnetic materials show that the damping frequency ν' is small compared with ν_n, and hence, from (44), the maximum absorption μ'' occurs when $\nu = \nu_n$. This result is of some importance in interpreting the observations on natural magnetic resonance.

8.4. Natural resonance in polycrystalline materials.

The conditions within an unmagnetised polycrystalline ferromagnetic material are much more complex than in a saturated material, in which the spins are all aligned in an unidirectional external field. The internal field H_n will vary in direction, due to local changes in the domain and crystalline structure, and it will also vary in magnitude, due to thermal and magnetic interactions. The polycrystalline material can, however, be considered as made up of small regions, of the order of the domain size or less, within which the internal field H_n is constant.

The contribution $[\chi/\chi_0]_N$ of each of these regions to the total relative susceptibility will be given by a relation similar to (42). $[\chi/\chi_0]_N$ depends on the local value of ν_n, but being a relative quantity, it is independent of the orientation of the region with respect to the high-frequency field. If the total number of such regions in unit volume is N, and the relative susceptibility of a number dN is $[\chi/\chi_0]_N$, then the total relative susceptibility will be given by

$$\chi/\chi_0 = \frac{1}{N} \sum [\chi/\chi_0]_N \, dN \qquad (45)$$

where the terms dN depend on the distribution of H_n, ν_n, and ν'.

If all interactions are neglected, and it is assumed that H_n is constant in magnitude throughout the polycrystalline material, and that ν' is also constant, then (45) reduces to (42). It has been found possible by a suitable choice of parameters, to obtain an approximate correlation with the observed polycrystalline dispersion and absorption

curves, using the simple damped resonance relation (42). Such a comparison with the measurements on magnetite is shown in Figure 18. This empirical correlation involves the selection of two parameters; ν_n which is taken from (43) as the frequency at which $\mu' = 1$, and ν', the damping frequency.

It is, however, necessary in each case to postulate a value of ν' greater than ν_n in order to account for the breadth of the observed absorption curves on this simple single-resonance theory. Such high damping coefficients are inconsistent with the data on induced magnetic resonance in ferromagnetic materials (§ 8.3.) which indicate that ν' is much less than ν_n. It appears more reasonable to consider alternatively that the broad natural magnetic resonances observed are due to a broad distribution of resonant frequencies about a mean value ν_{n_0}, corresponding to the un: :disturbed or unicrystalline anisotropy

field H_{r_0} . On this model, the polycrystalline resonance is made up of a broad series of relatively sharp resonances, occurring locally in individual domains. In the absence of any suitable theory for treating the thermal and long-range magnetic interactions responsible for the distribution of H_r about H_{r_0}, no attempt has been made to develop (45) to obtain a detailed dispersion relation. The mean resonant wavelength λ_{r_0} can, however, be derived directly from the observations as the wavelength at which the magnetic absorption μ'' is a maximum; (cf. § 8.3.). The values of λ_{r_0} and H_{r_0} obtained for the different solid materials are given in Table 8.

Evidence in favour of the distributed-resonance theory is provided by the observations on the effect of an applied field on the dispersion (Fig.9). Apart from the shift of the resonance towards higher frequencies, due to the

Table 8 - Resonance parameters and fields.
(Distributed - resonance theory).

Material	λ_{n_0} (cm.)	ν_{n_0} (Mc/s)	H_{n_0} (gauss)
γ -ferric oxide	40	750	268
Magnetite	18	1670	595
Mn Zn ferrite	70	430	153
Ni Zn ferrite	50	600	214

increase of the effective field acting on the spins, there is a reduction in the width of the resonance, corresponding to the decrease in magnetic disorder in the material as the domain moments are turned from random orientations towards the direction of the applied field.

9. THE INTERNAL ANISOTROPY FIELD.

9.1. Anisotropy energy and the internal field.

The anisotropic properties of a ferromagnetic material are normally described in terms of an anisotropy energy coefficient, K (Bitter, 1937). For a cubic crystal, magnetised to saturation, the component of the magnetic energy due to anisotropy may be formally expressed as

$$f = K\left(\alpha_1^2\alpha_2^2 + \alpha_2^2\alpha_3^2 + \alpha_3^2\alpha_1^2\right) \qquad (46)$$

where $\alpha_1, \alpha_2, \alpha_3$, are the direction cosines of the magnetisation relative to the cube edges, the (100) axes. The value of K, the anisotropy energy coefficient, can be derived experimentally from the difference between the energies of magnetisation of the crystal along the different crystal axes, since from (46)

$$f_{111} - f_{100} = K/3 \qquad (47)$$

$$f_{110} - f_{100} = K/4 \qquad (48)$$

Quittner (1909) has measured the magnetisation curves of a magnetite crystal along its three crystallographic axes. Magnetite, like the other compounds studied, has a spinel-type cubic structure, and its preferred direction of magnetisation is along the cube diagonal, or (111) axis. Comparison of the relations (47) and (48) with Quittner's measurements gives a value of $K = -1{\cdot}124 \times 10^5$ ergs./cc., for magnetite.

The internal anisotropy field H_{a_0} in a crystal can be simply related to the anisotropy energy coefficient K, and the saturation intensity M. Let us consider a single domain of a cubic crystal, lying in a [100] plane Oyz, whose easy direction of magnetisation lies along a (100) axis, Oz (Figure 19). In the unmagnetised state M is directed along Oz, and the internal field H_{a_0} acts in the same direction. If now a small transverse field H_x is applied along Ox, M will be rotated through a small angle θ

in the [100] plane Oxz, where

$$\tan\theta = \frac{H_x}{H_{k_0}} \qquad (49)$$

The internal field H_{k_0} exerts a restoring torque on M, given by

$$T = M H_{k_0} \sin\theta \qquad (50)$$

Alternatively, if the process is described in terms of the anisotropy energy f (46), we have in the plane Oxz, $\alpha_1 = \sin\theta$, $\alpha_2 = 0$, $\alpha_3 = \cos\theta$, so that f reduces to

$$f = K \cos^2\theta \sin^2\theta \qquad (51)$$

The anisotropy energy exerts a restoring torque

$$T = \frac{\partial f}{\partial \theta} = K \sin 2\theta \cos 2\theta \qquad (52)$$

Equating the torques (50) and (52), we obtain

$$H_{k_0} = \frac{2K}{M} \cos\theta \cos 2\theta \qquad (53)$$

which, for θ small, reduces to

$$H_{k_0} = \frac{2K}{M} \qquad (54)$$

(54) gives the effective anisotropy field for a cubic crystal, in which the (100) axes are

the preferred magnetisation directions.

The corresponding case for a crystal in which the (111) axes are preferred, can be obtained in a similar manner, by expressing the anisotropy energy f in terms of a second anisotropy coefficient K', such that

$$f = K'(\alpha_1'^2\alpha_2'^2 + \alpha_2'^2\alpha_3'^2 + \alpha_3'^2\alpha_1'^2) \quad (55)$$

where α_1', α_2', α_3', are the direction-cosines of the magnetisation, relative to the (111) axes. The analysis then follows identical lines to that given above, and we obtain

$$H_{n_0} = \frac{2K'}{M} \quad (56)$$

Since from (55), the difference in anisotropy energies along the (100) and (111) axes is

$$f_{100} - f_{111} = K'/3 \quad (57)$$

we have, by comparison with (47), that $K' = -K$, and hence (56) becomes

$$H_{n_0} = -\frac{2K}{M} \quad (58)$$

Thus, for both the (100) and (111) axes, we obtain for the magnitude of the anisotropy field

$$H_{n_0} = \frac{2|K|}{M} \qquad (59)$$

This relation has been compared with the data on magnetite. The saturation intensity of artificial magnetite at room temperature, $M = 450$ (Weiss and Forrer, 1929), so that combining this with the value of $K = -1{\cdot}124 \times 10^5$ from Quittner's data, we obtain from (58), that $H_{n_0} = 500$. This value agrees satisfactorily with that of $H_{n_0} = 595$, obtained from the peak of the natural magnetic absorption.

No data is available on the magnetic properties of single crystals of the other compounds studied. The magnitude of the anisotropy constant K can, however, be estimated from H_{n_0}, provided the saturation intensity M is known. The sign of K will depend on whether the (111) or (100) axes are the preferred magnetisation directions. Weiss and

Forrer (1929) have obtained $\sigma = 76{\cdot}0$ for the specific saturation intensity of γ - ferric oxide at room temperature. The density of the solid material used in the present investigation is 4·65 gm./cc., and, hence, $M = 354$. Combining this with the value of H_{k_0} from Table 8 , we obtain, from (59)

γ -ferric oxide : $|K| \sim 4{\cdot}7 \times 10^4$ ergs./cc.

A saturation intensity of $M = 200$ has been observed by Hewitt (1948) for a specimen of manganese-zinc ferrite, so that, assuming a similar value for the material used, we find

Mn-Zn ferrite : $|K| \sim 1{\cdot}5 \times 10^4$ ergs./cc.

There appears to be no published data on the saturation intensity of nickel-zinc ferrite, but taking an approximate value of $M \sim 300$, gives

Ni-Zn ferrite : $|K| \sim 3{\cdot}2 \times 10^4$ ergs./cc.

The magnitude of K is one of the principal factors determining the initial permeability of a ferromagnetic material, a small anisotropy being associated with a

large initial permeability (Snoek 1947a). In Table 9, the derived values of $|K|$ and μ_o, the initial rotational component of permeability, are compared. It will be observed that $|K|$ and μ_o are in inverse sequence, as it is to be expected.

9.2. The internal field and the initial permeability.

Although the quantitative results obtained for the four compounds studied depend on the exact composition of the particular specimens used, comparison of the initial permeabilities μ_s from Table 7 with those from other sources (Table 10) indicates that, with the exception of the manganese-zinc ferrite, the specimens are representative.

It appears, however, that the composition of the manganese-zinc ferrite specimen differs appreciably from the optimum mixtures obtained by Snoek (1947a, 48) which have $\mu_s \sim \mu_o \sim 1000$. In such materials, the value of $|K|$ will be much smaller, and, consequently, natural magnetic resonance

Table 9. - Anisotropy coefficient K and μ_o.

Material	$\lvert K \rvert$	μ_o
Magnetite	$11{\cdot}2 \times 10^4$	8
γ-ferric oxide	$4{\cdot}7 \times 10^4$	30
Ni Zn ferrite	$3{\cdot}2 \times 10^4$	34
Mn Zn ferrite	$1{\cdot}5 \times 10^4$	44
Mn Zn ferrite; obtained from data of Snoek (1948), (see § 9.2)	$0{\cdot}7 \times 10^3$	~1000

Table 10. - Comparison of μ_s with published data.

Material	(Table 7) μ_s	(Publ.) μ_s	Source
Magnetite	15	~ 17	Kittel (1946)
γ-ferric oxide	34	~ 31	Welo and Baudisch (1925)
Ni Zn ferrite	40	~ 50	Snoek (1947a)
Mn Zn ferrite	48	~1000	Snoek (1947a)

should occur at much lower frequencies. Snoek (1948) has observed the initial part of a sharp rise in the magnetic absorption of optimum manganese-zinc ferrite mixtures at frequencies below .1 Mc/s. This is interpreted by Snoek as the fringe of a magnetic resonance region, but his observations have been confined to frequencies well below the natural resonance frequency. From the limited data, it may be estimated that this occurs at about 20 Mc/s, which is equivalent, on the theory given in § 9.1., to an internal field $H_{i_0} \sim$ 7 gauss, and $|K| \sim$ 700 ergs./cc.

The simple domain model, considered in § 9.1., has been used by Snoek (1948), to obtain a relation between the transverse susceptibility χ_x, and the internal field H_{i_0}. We have, referring to Figure 19,

$$\chi_x = \frac{M \sin\theta}{H_x} = \frac{M\cos\theta}{H_{i_0}} \qquad (60)$$

so that for the initial susceptibility,

where θ is small,

$$\chi_\chi = \frac{M}{H_{n_0}} \qquad (61)$$

Combining this with (59), a simple relation for χ_χ in terms of $|K|$ and M is obtained,

$$\chi_\chi = \frac{M^2}{2|K|} \qquad (62)$$

If the applied field is not normal, but makes an angle ϕ with the direction of M, then since only its transverse component causes rotational magnetisation, the rotational susceptibility

$$\chi_\phi = \chi_\chi \sin^2\phi \qquad (63)$$

For a polycrystalline material, containing N domains per unit volume, of which a number dN have a rotational susceptibility χ_ϕ, the mean rotational susceptibility will be

$$\chi_0 = \frac{1}{N} \sum \chi_\phi \, dN \qquad (64)$$

where the terms dN depend on the distribution of χ_χ, which is governed by the local internal field, and of ϕ, which is random. If it is assumed, for simplicity, that χ_χ is

constant, i.e. that the local internal field is constant in magnitude, then (64) becomes

$$\chi_0 = \frac{\int_0^{\pi} \chi_\chi \sin^3\phi \, d\phi}{\int_0^{\pi} \sin\phi \, d\phi} = \frac{2}{3}\chi_\chi \qquad (65)$$

Hence, from (61)

$$H_{h_0} = \frac{2}{3}\frac{M}{\chi_0} = \frac{8\pi M}{3(\mu_0 - 1)} \qquad (65)$$

so that for a given value of M, the internal field H_{h_0} should be inversely proportional to $\mu_0 - 1$.

The parameters derived from Sneek's measurements on the manganese-zinc ferrite specimen, $\mu_0 \sim 1000$, have been compared with those obtained for the specimen, $\mu_0 = 44$. It is found that the values of H_{h_0} are $\sim$ 1 : 22, while those of $\mu_0 - 1$ are $\sim$ 23 : 1. Thus, the relative magnitudes of the internal fields and the anisotropy coefficients are accounted for by the difference in the initial permeabilities of the two specimens.

In Table II, the theoretical values of H_{h_0} derived from (65) are compared with those obtained experimentally from the

Table 11 - Comparison of H_{π_0} with theory (65)

Material	H_{π_0} (exptl.)	H_{π_0} (theor.)	$\frac{H_{\pi_0}(exp.)}{H_{\pi_0}(th.)}$	μ_0
Magnetite	595	540	1·1	8
ɣ-ferric oxide	268	100	2·7	30
Ni Zn ferrite	214	74	2·9	34
Mn Zn ferrite	153	42	3·6	44

magnetic absorption maxima. In the case of magnetite, there is a reasonably close agreement between the two values, but for the other materials, there is a discrepancy by a factor ~ 3. A similar discrepancy has been found by Snoek (1947[b]) in comparing a relation, based on (65) with his observations on an unspecified ferrite material. Nevertheless, the order of agreement is sufficiently close to provide a further verification of the nature of the dispersion process, as the resonance of the spin rotations in the internal field. The discrepancy increases with μ_0, and it can be readily attributed to the magnetic interactions between domains, which have been neglected in the derivation of (65).

10. CONCLUSION.

The principal results of the research described in this thesis may be summarised as follows.

A waveguide impedance method has been developed for measuring the magnetic and dielectric properties of low-conductivity materials at high frequencies. Coaxial-line and H_{10} waveguide apparatus has been constructed, and operated in the microwavelength region from 60 cm. to 1·23 cm. Suitable techniques have been evolved for the precise measurement of the stationary wave patterns, from which the input impedances and electromagnetic properties of the materials are computed.

Observations have been made on a series of mixtures containing various ferromagnetic compounds; γ-ferric oxide, magnetite, manganese-zinc ferrite, and nickel-zinc ferrite. From these observations, the high-frequency properties of the solid compounds have been obtained by extrapolation. Each of the materials has a pronounced magnetic dispersion and absorption in the microwave region. When a static magnetic field is applied, this dispersion shifts towards higher frequencies and becomes sharper.

Analysis of the observations has led to the following conclusions.

(a) The dominant magnetisation process in low-conductivity ferromagnetic materials is the rotation of the spin-moments within the domains towards the direction of the applied field. The translational magnetisation component is relatively small, and decays at frequencies below the microwave region. Irreversible effects also disappear at low frequencies.

(b) The observed dispersion is due to the decay of the rotational magnetisation component. This occurs as a natural resonance process, corresponding to the Larmor precession of the electronic spin-moments in the internal field of the ferromagnetic material.

(c) A distribution of the values of this internal field about a mean field H_{n_0} leads to a broad distribution of resonant frequencies about a mean frequency ν_{n_0}.

(d) The internal field arises from the magnetic anisotropy of the material. In magnetite, the value of H_{i_0} derived from the peak absorption frequency agrees closely with the effective anisotropy field, obtained from crystalline magnetisation data. In the other materials, the magnitude of the anisotropy constant K has been estimated from H_{i_0} and the saturation intensity M .

(e) The internal field also determines the static rotational magnetisation of the material, and a reasonable correlation has been obtained between H_{i_0} and μ_0 , the initial rotational permeability. The occurrence of natural magnetic resonance at much lower frequencies in high-permeability materials is thus explained.

11. PUBLICATIONS.

The following papers, published by the author, deal with various aspects of the work described in the present thesis.

1946 a "Dielectric housings for centimetre wave antennae" J.I.E.E. 93 (III A), 647.

1946 b "Magnetic dispersion of iron oxides at centimetre wavelengths", Nature, 158, 671.

1947 a "Magnetic dispersion of δ-ferric oxide", Nature, 159, 775.

1947 b "Mechanism of ferromagnetic dispersion", Nature, 160, 535.

1948 a "The measurement of the permeability of low-conductivity ferromagnetic materials at centimetre wavelengths". Proc. Phys. Soc. 60, 282.

1948 b "Microwave magnetic dispersion in carbonyl iron powder". Phys. Rev. 74, 843.

1949 "The Physical applications of microwaves", J. Brit. I.R.E. 9, 10.

A further paper dealing in more detail with the dispersion of the ferromagnetic compounds is yet to be published.

12. REFERENCES.

Allanson (1945) J.I.E.E. III, 92, 247.

Arkadiew (1913) Phys. Zeit. 14, 928.

Arkadiew (1914) Ann. der Phys. 45, 133.

Arkadiew (1919) Ann. der Phys. 58, 105.

Arkadiew (1924) Ann. der Phys. 75, 426.

Arkadiew (1926) Ann. der Phys. 81, 649

Arkadiew (1945) J. Phys. USSR. 9, 373.

Becker (1938) Zeit. f. Tech. Phys. 19, 542.
Phys. Zeit. 39, 856.

Becker and Doring (1939) "Ferromagnetismus" (Springer).

Bitter (1937) "Introduction to Ferromagnetism" (McGraw-Hill)

Buchner (1939) Wiss. Veroff, a.d. Siemens-Werken, 18, 84.

Collie, Ritson and Hasted (1946) Trans. Far. Soc. 42A, 129.

Cummerow and Halliday (1946) Phys. Rev. 70, 433.

Dannatt (1936) J.I.E.E. 79, 667.

Debye (1929) "Polar Molecules" (Chem.Cat.Co.)

Epelboim (1947) J. de Phys. et Rad. 8, 251.

Foster and Newlon (1941) Proc. I.R.E. 29, 266.

Frenkel (1945) J. Phys. USSR. 9, 229.

Gans and Loyarte (1921) Ann. der Phys. 64, 209

Glathart (1939) Phys. Rev. 55, 833.

Gorter (1947) "Paramagnetic Relaxation" (Elsevier).

Griffiths (1946) Nature, 158, 670.

Guillien (1941) Ann. de Phys. 16, 205.

Hagen and Rubens (1903) Ann. der Phys. 11, 873.

Hewitt (1948) Phys. Rev. 73, 1118.

Hoag and Cox (1940) Phys. Rev. 58, 203.

Hoag and Gottlieb (1939) Phys. Rev. 55, 410.

Hoag and Jones (1938) Phys. Rev. 42, 571.

Israel (1926) Zeit. f. Phys. 39, 855.

Johnson, Rado and Maloof (1947) Phys. Rev. 71, 322.

Kartschagin (1922) Ann. der Phys. 67, 325.

Kennelly (1914) "Chart Atlas of Complex Hyperbolic and Circular Functions" (Harvard Univ. Press).

King (1955) Proc. I.R.E. 43, 926.

Kittel (1946) Phys. Rev. 70, 281.

Kittel (1947) Phys. Rev. 71, 270.

Kittel (1948) Phys. Rev. 73, 155.

Kreielsheimer (1933) Ann. der Phys. 17, 293.

Landau and Lifshitz (1935) Phys. Z. Sowjetunion, 8, 153.

Legg and Given (1940) Bell Syst. Tech. J. 19, 385.

Lichtenecker (1918) Phys. Zeit. 19, 374.

Lindman (1938) Zeit. f. Tech. Phys. 19, 323.

MacFarlane (1945) Ministry of Supply, SIGESO Report.

Michels (1931) Ann. der Phys. 9, 877.

Mohring (1939) Hft. u. Elak, 53, 196.

Potapenko and Sanger (1933) Naturwiss, 21, 818.

Potapenko and Sanger (1937) Zeit. f. Phys. 104, 779.

Procupiu and d'Albon (1937) Comptes Rendus, 205, 1373.

Schelkunoff (1938) Bell Syst. Tech. J. 17, 17.

Schmidt (1948) App. Sci. Res. B1, 127.

Schwarz (1932) Zeit. f. Hft. 39, 160.

Simon (1946) Nature, 157, 735.

Snoek (1947a) "New developments in ferromagnetic materials" (Elsevier).

Snoek (1947b) Nature 160, 90.

Snoek (1948) Physica 14, 207.

Strutt (1931) Zeit. f. Phys. 68, 632.

Volkova (1932) Zeit. f. Phys. 74, 388.

Wait (1927) Phys. Rev. 29, 566.

Webb (1938) Proc. I.R.E. 26, 433.

Welo and Baudisch (1925) Phil. Mag. vi, 50, 399.

Wien (1931) Ann. der Phys. 8, 899; 11, 423; 11, 736.

Woods (1942) J. App. Phys. 13, 314.

Wul (1946) J. Phys. USSR. 10, 95.

Yager and Bozorth (1947) Phys. Rev. 72, 80.

Zavoisky (1946) J. Phys. USSR. 10, 197.

Zimowski (1937) Acta Physica Polonica, 6, 6.

Figure 1. Collected experimental data on high-frequency permeability (μ_R and μ_L) of Iron.

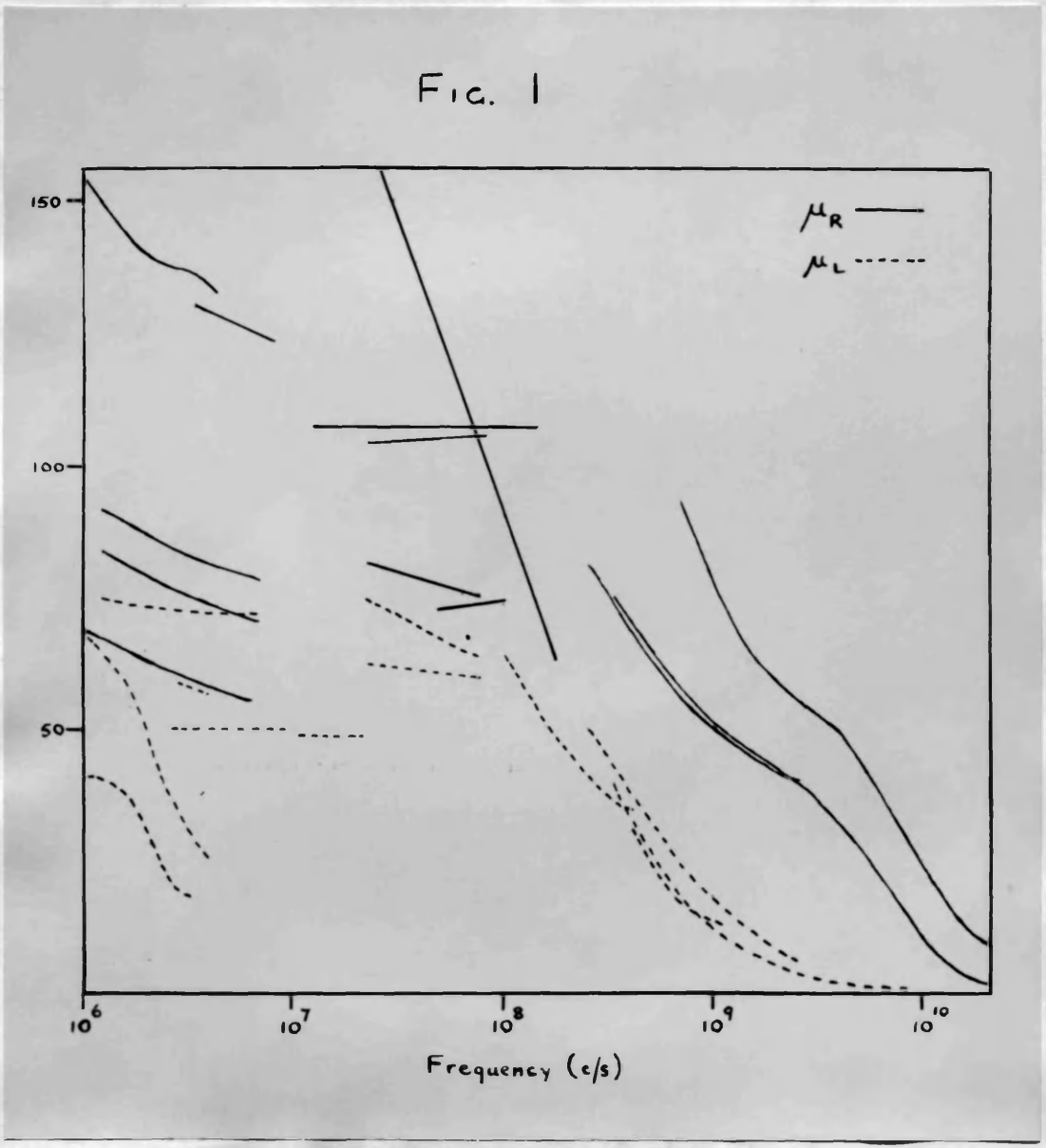

Figure 2. General schematic diagram of waveguide impedance apparatus.

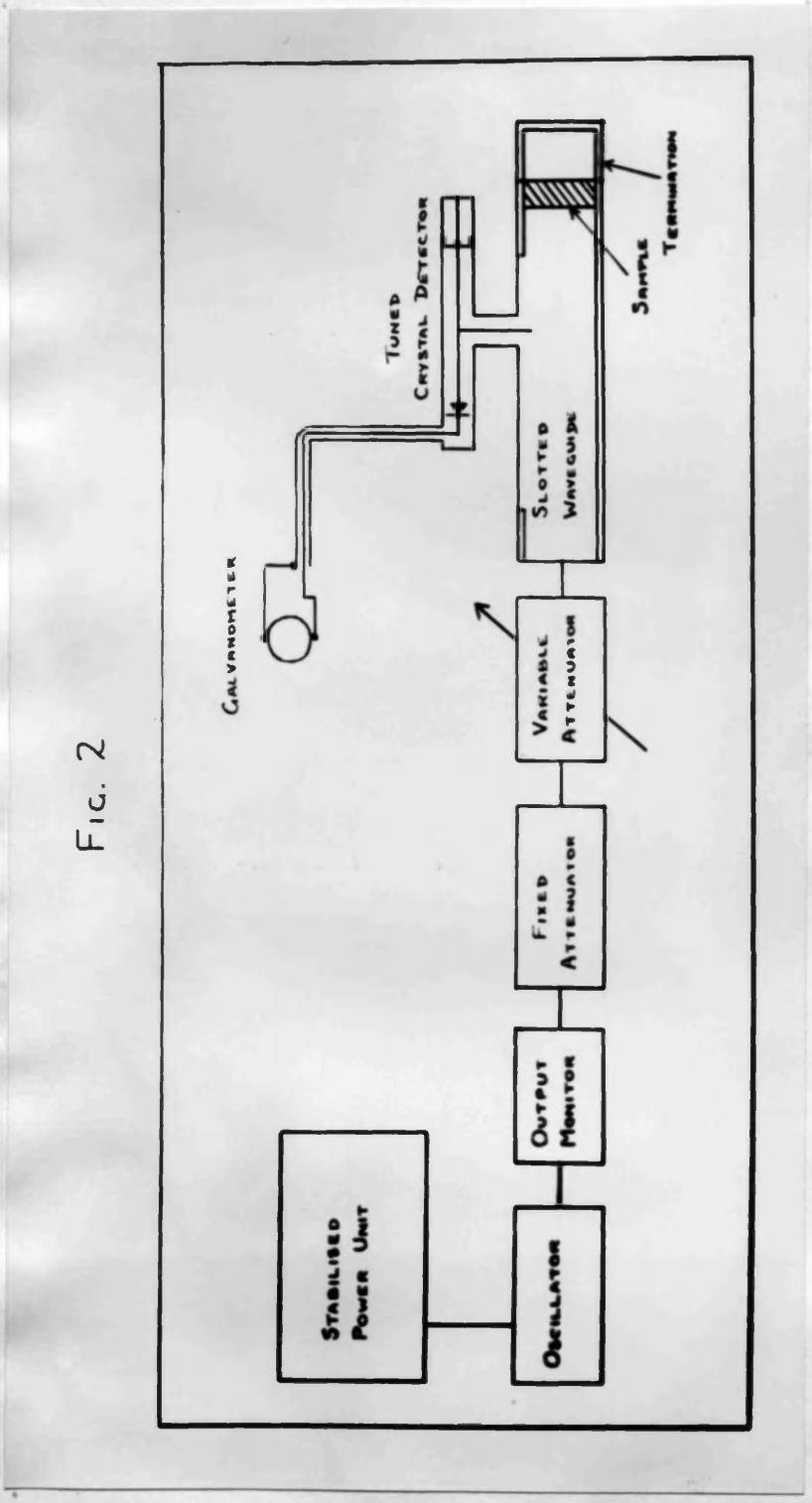

Fig. 2

Figure 3. Broad-band reflex klystron oscillator.

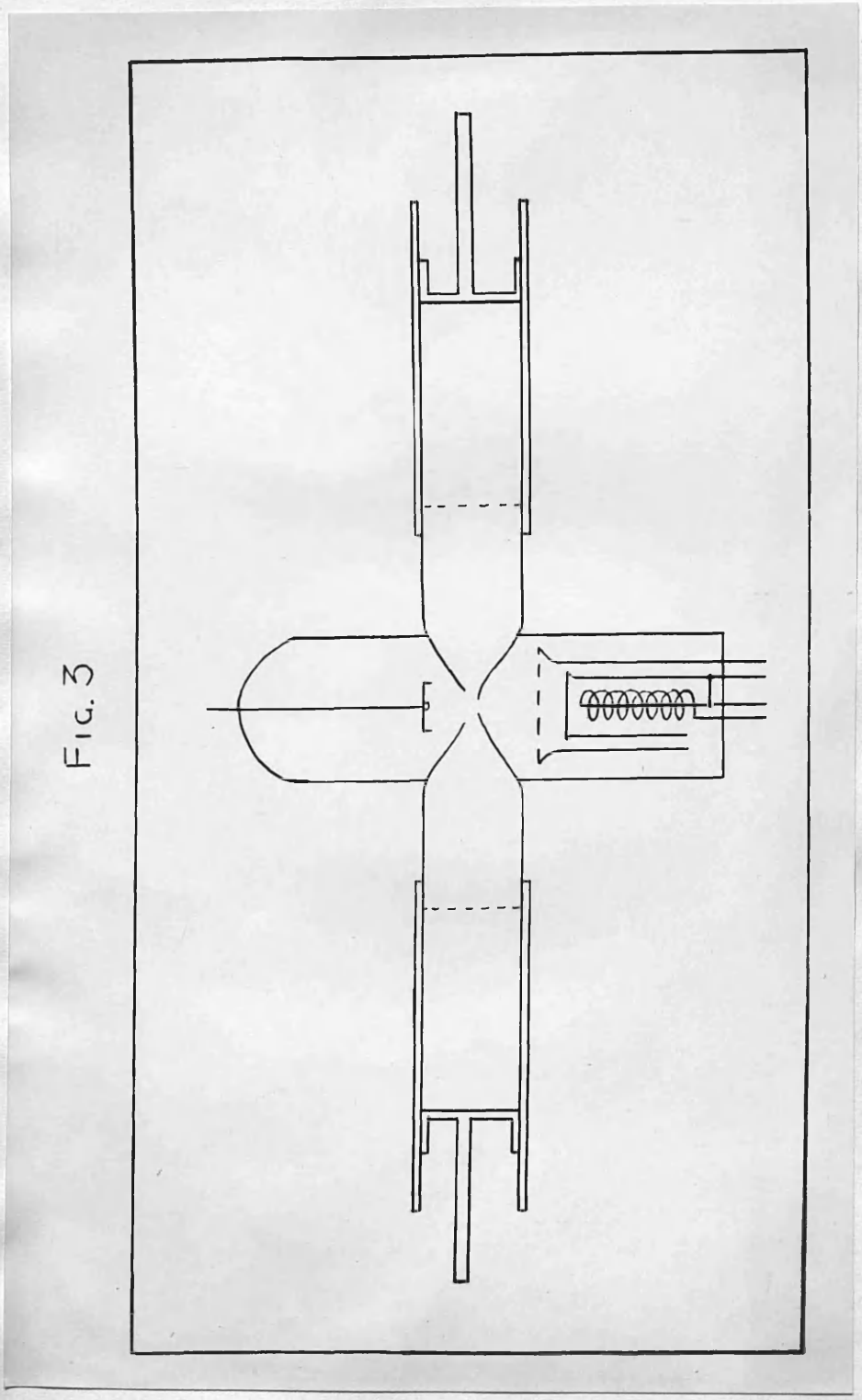

Figure 4. Calibration curves for typical crystal. Dependence on circuit resistance, R .

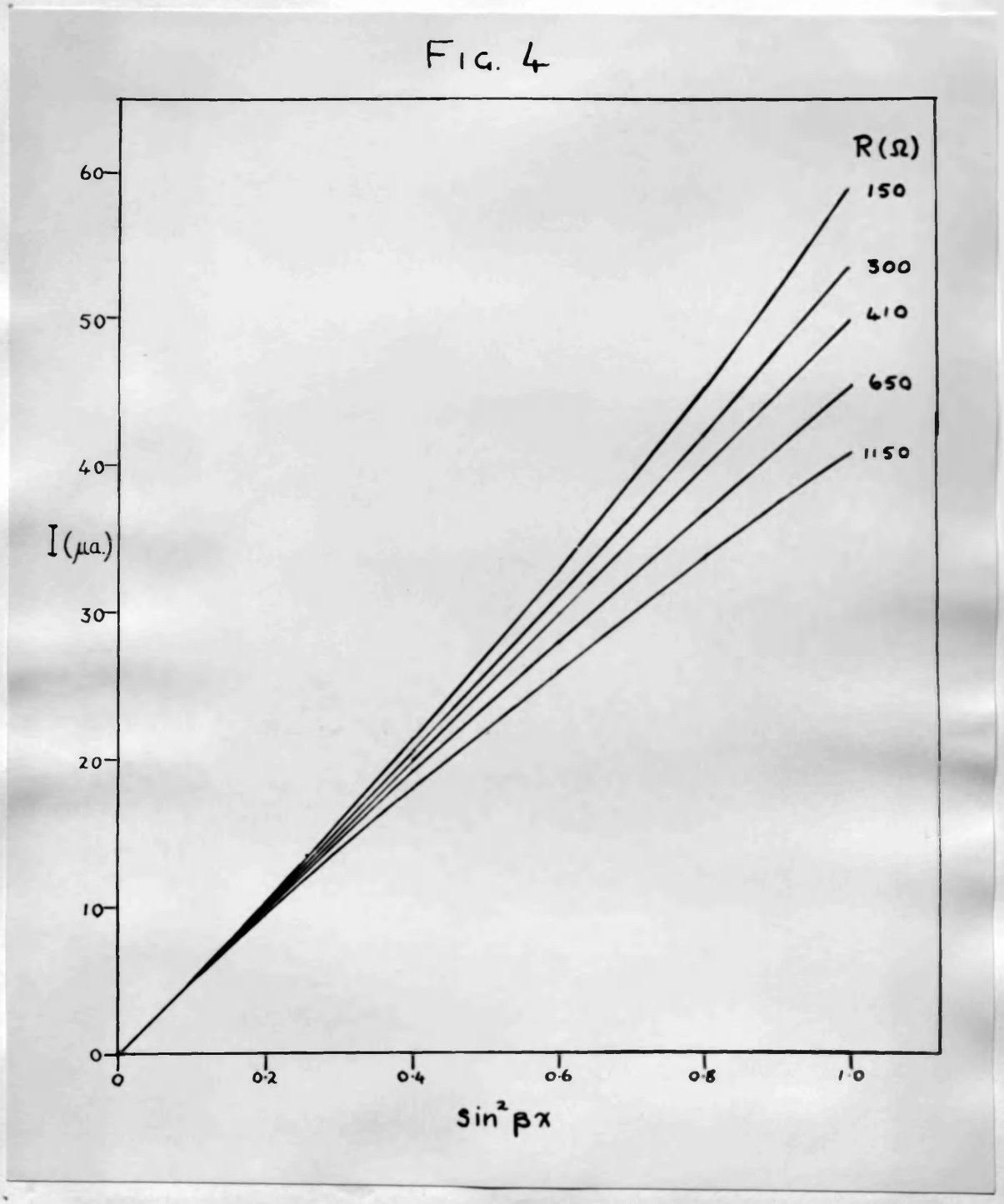

Figure 5. Standing-wave measurement.

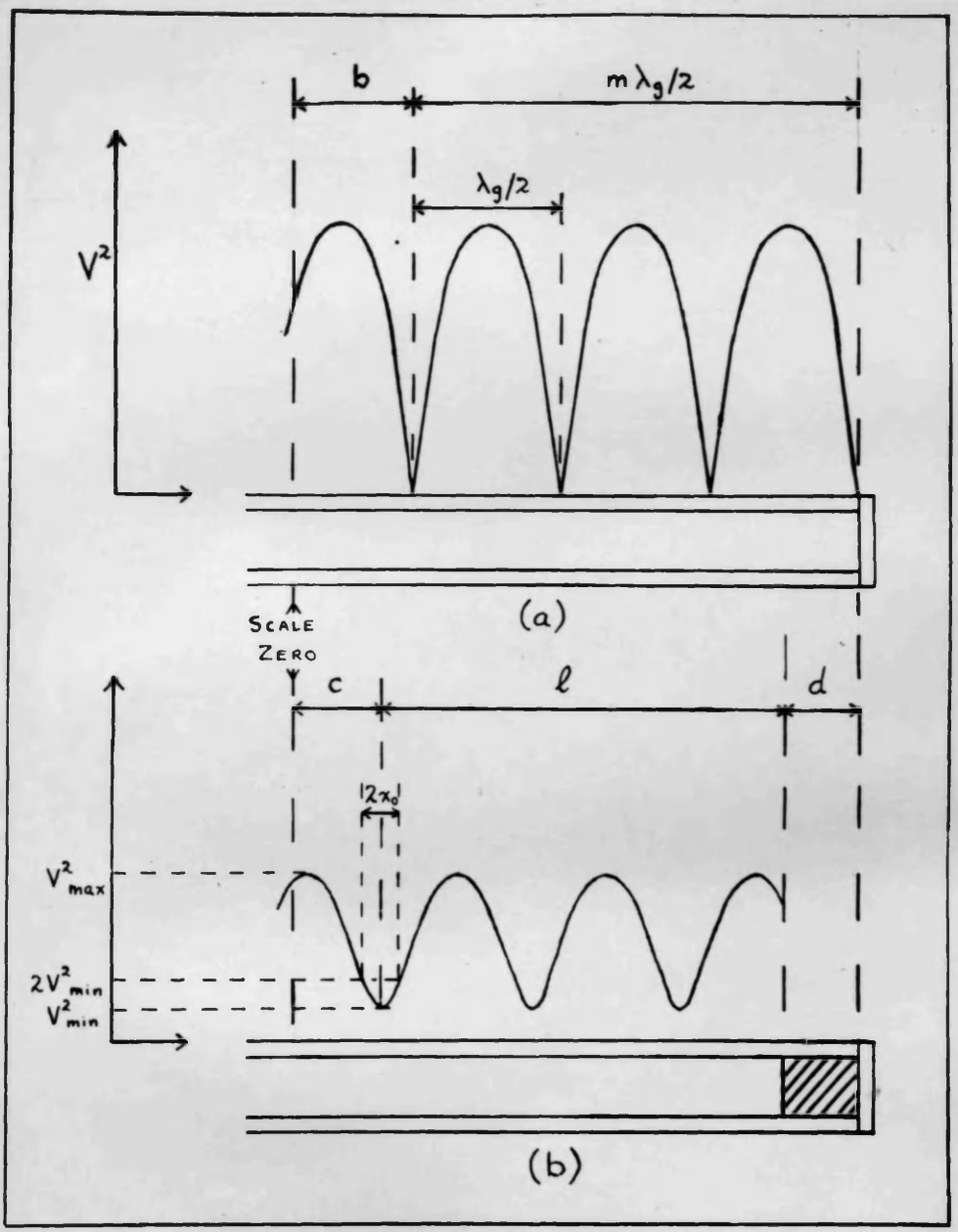

FIG. 5

Figure 6. Magnetic dispersion and absorption of 32·6% γ -ferric oxide mixture.

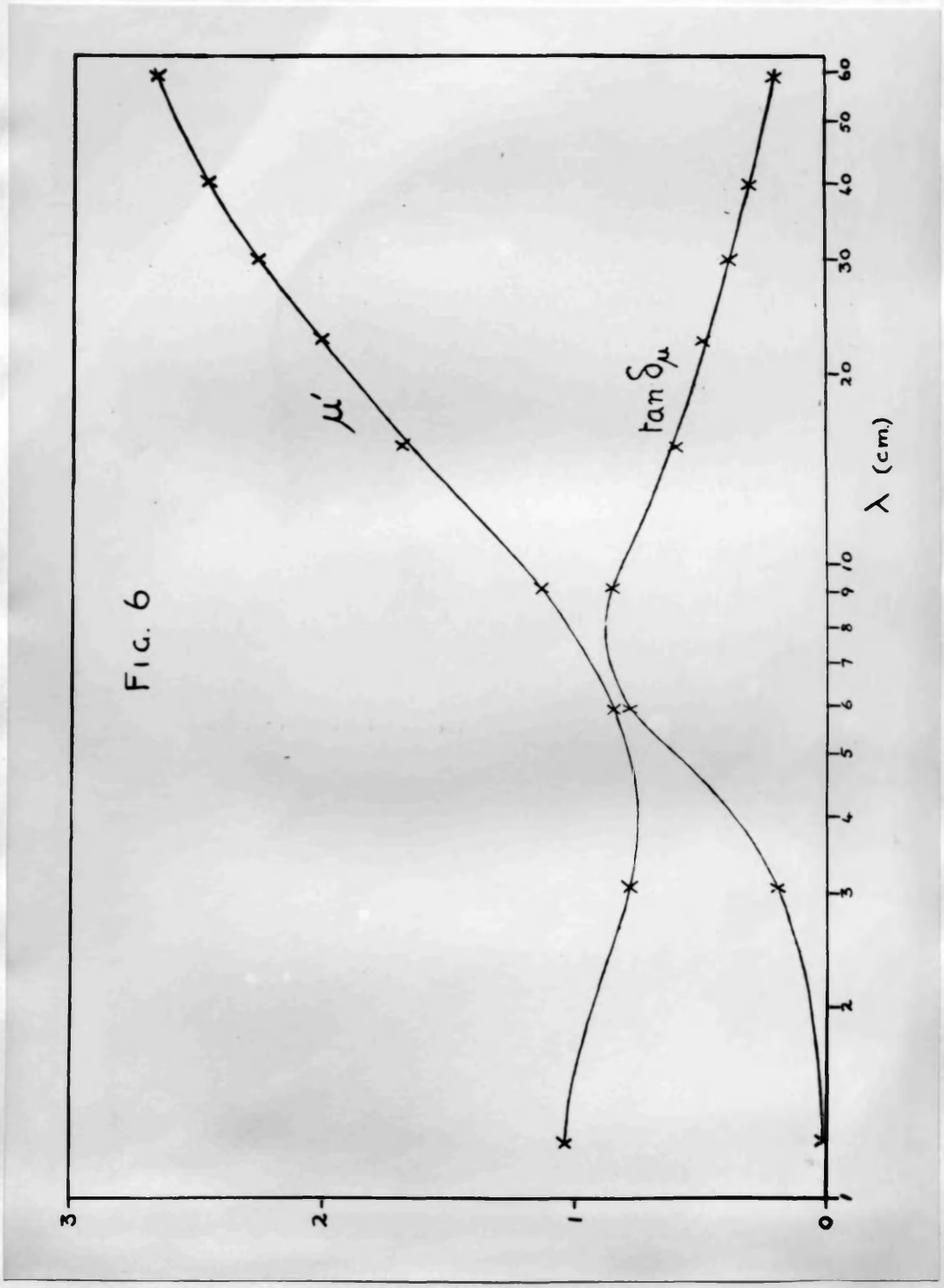

Figure 7. Dielectric dispersion and absorption of 32·6% γ-ferric oxide mixture.

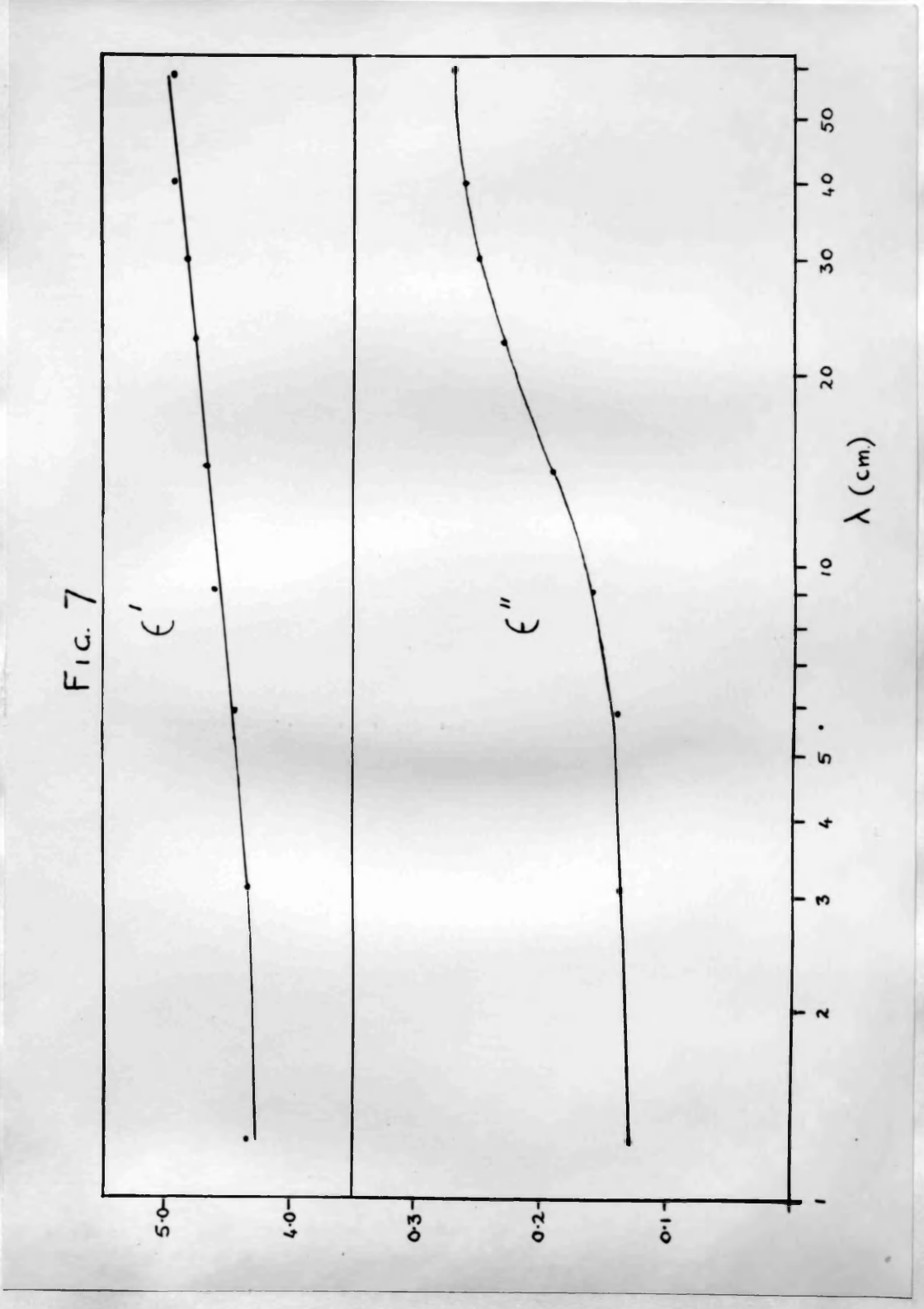

Figure 8. Effect of applied field H on high-frequency permeability.

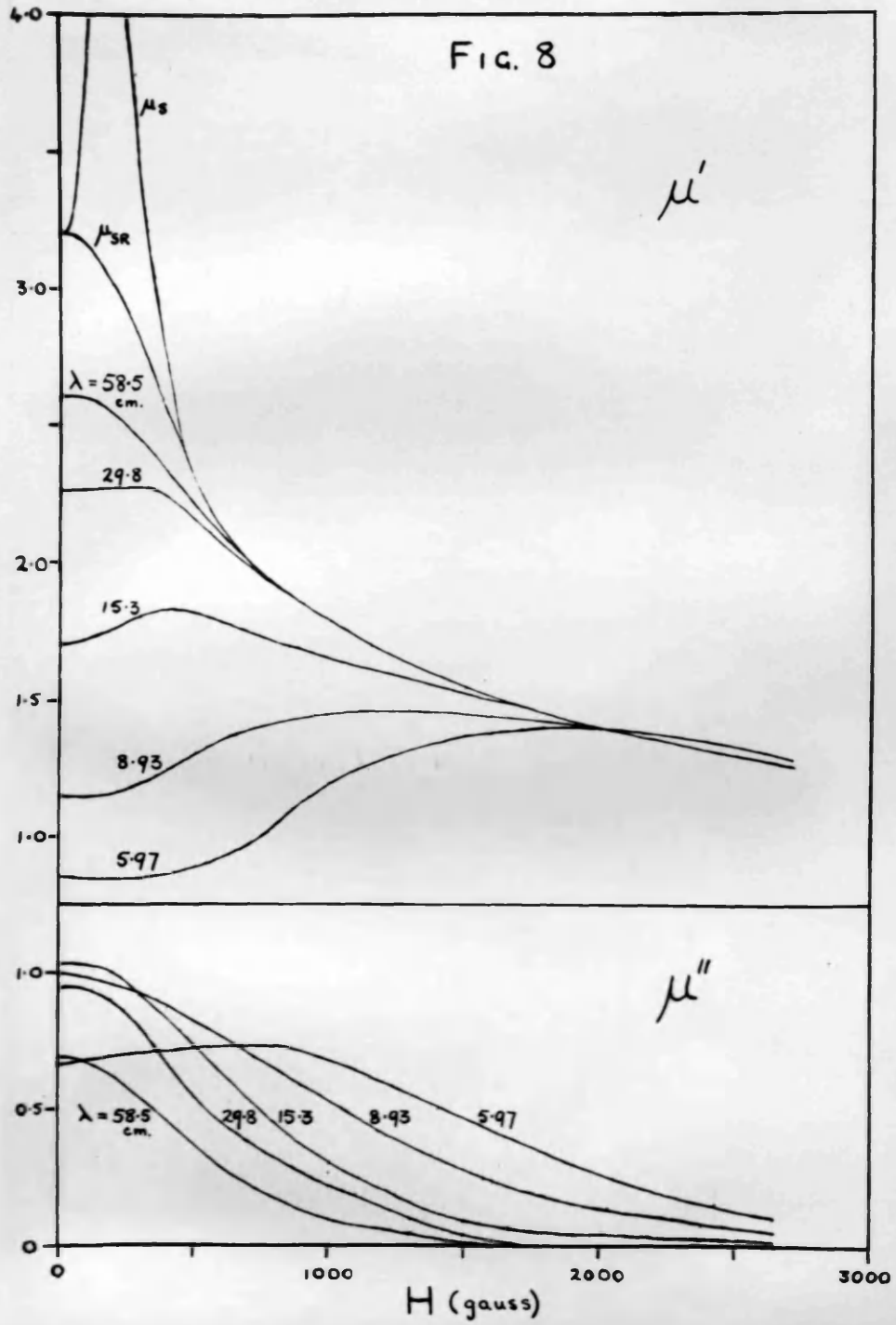

Figure 9. Effect of applied field H on relative magnetic dispersion and absorption.

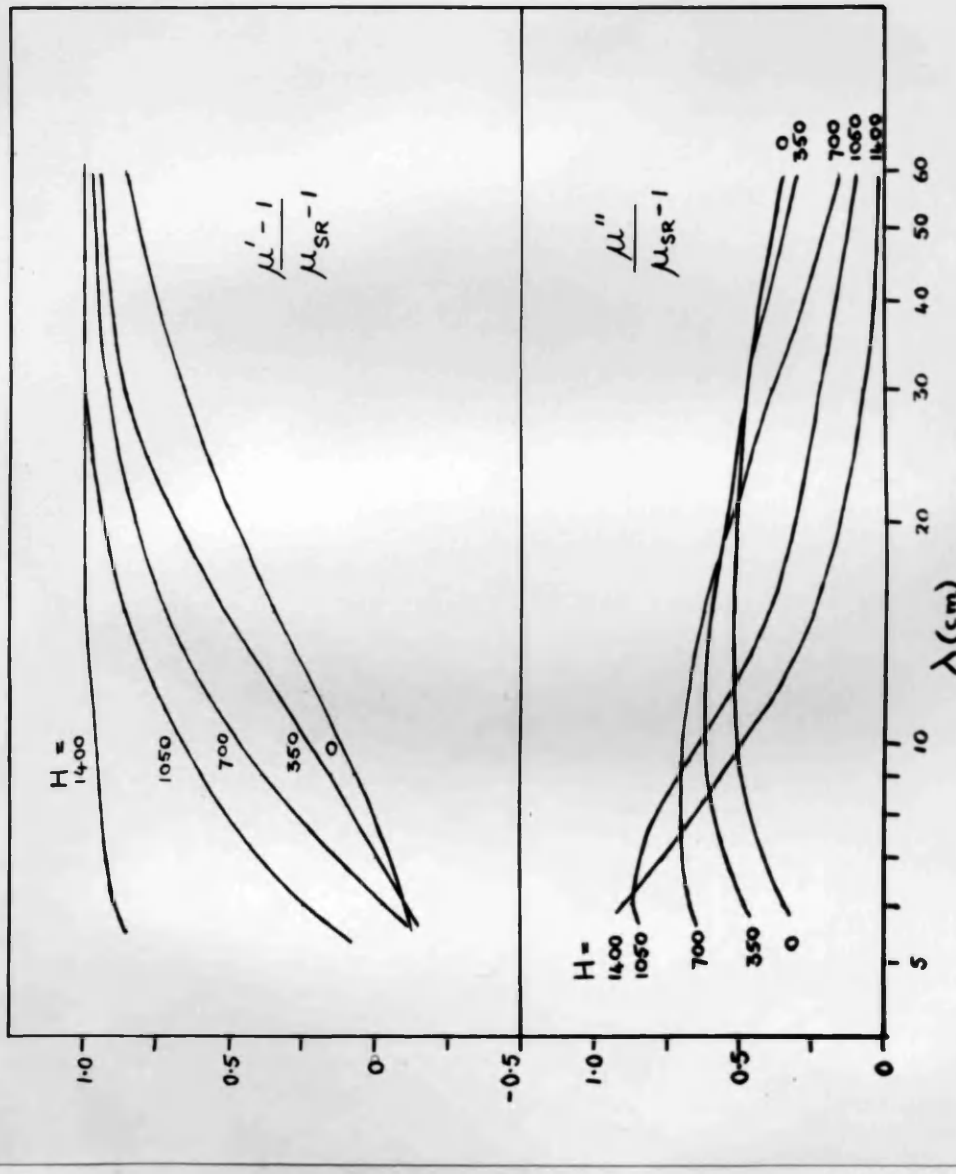

FIG. 9

Figure 10. δ -ferric oxide mixtures. Dependence of $|\mu|$ on concentration v, at different wavelengths

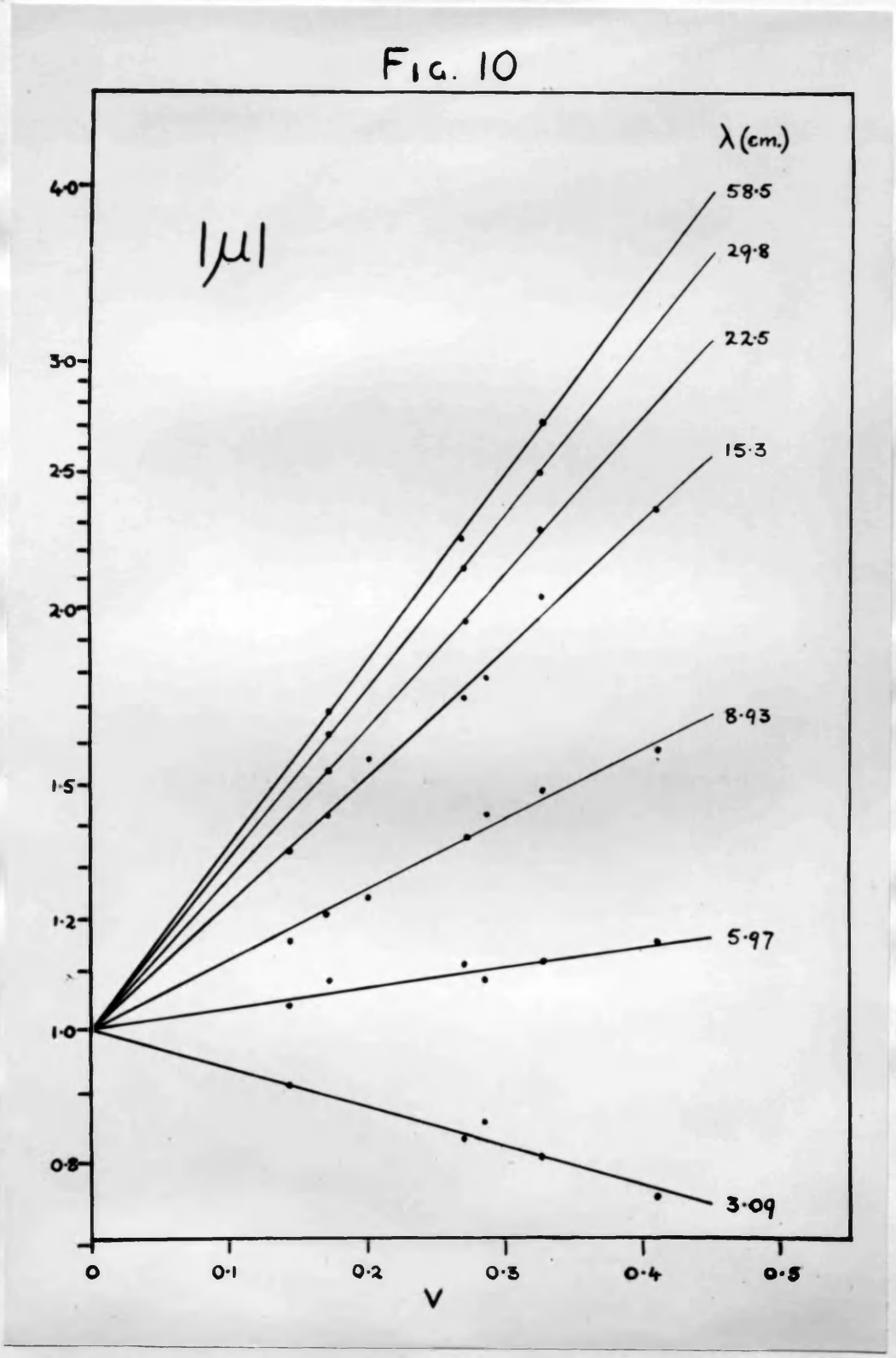

Figure 11. δ-ferric oxide mixtures. Dependence of magnetic loss tangent on concentration v.

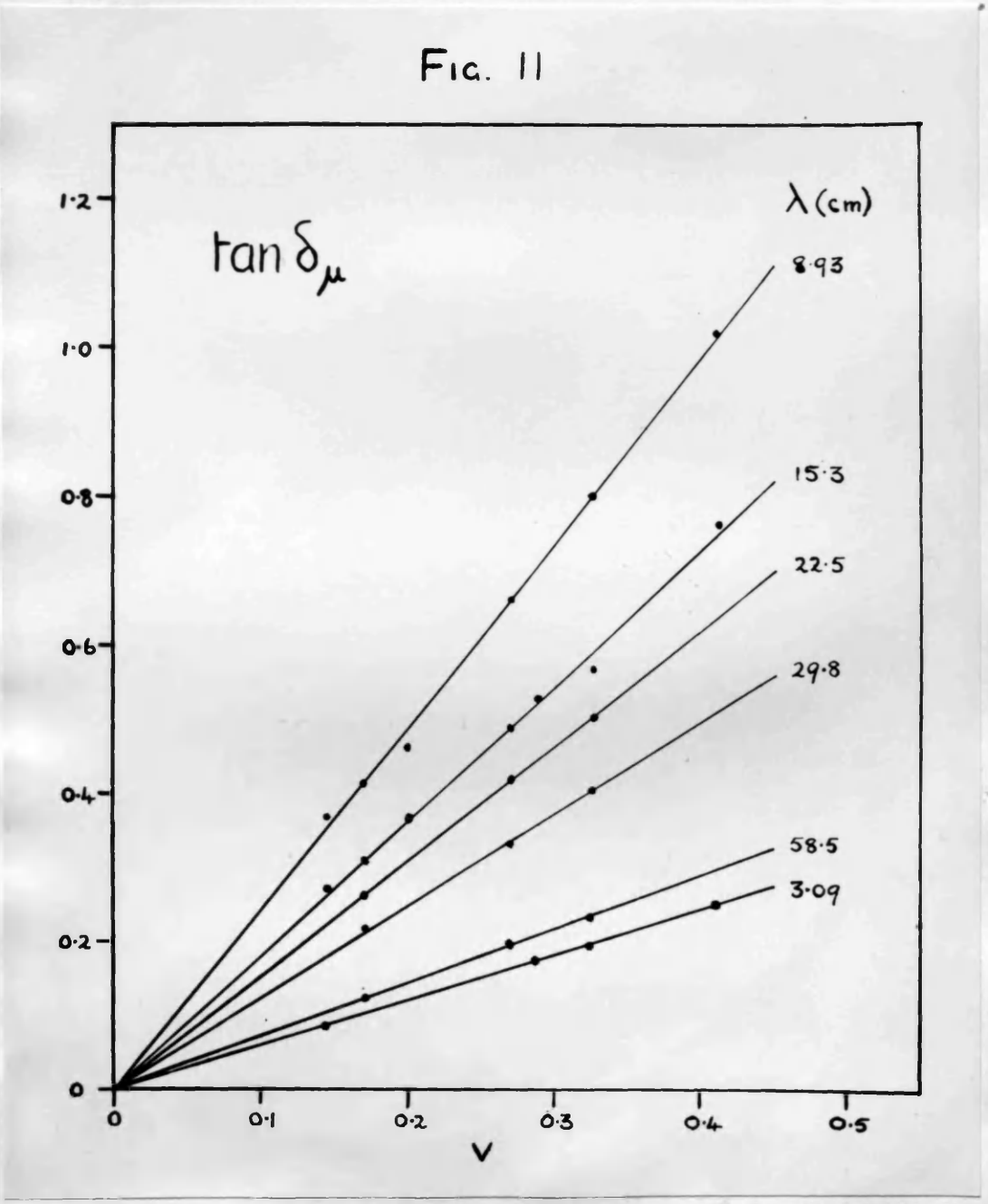

Figure 12. Magnetic dispersion and absorption of γ-ferric oxide.

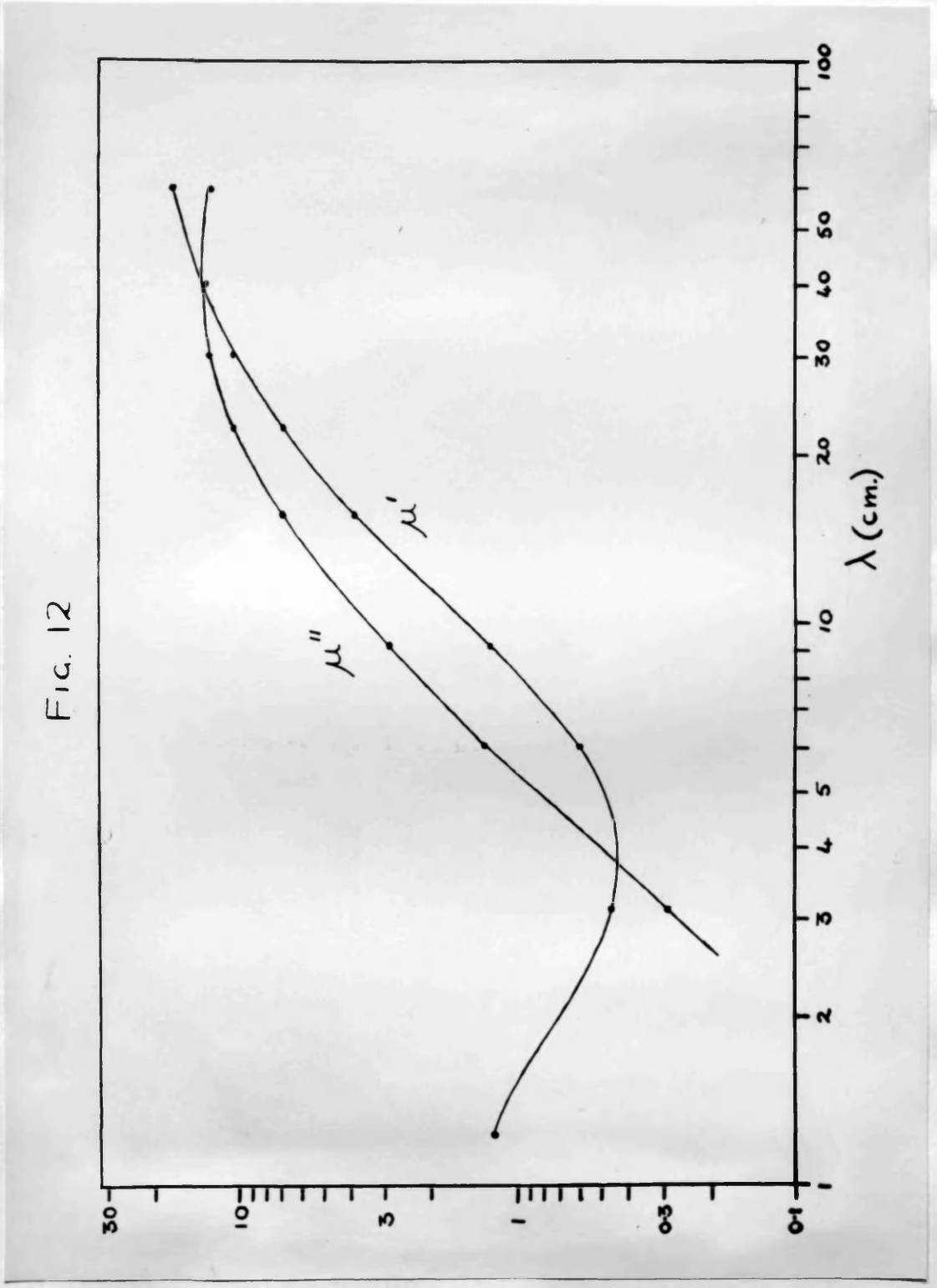

Figure 13. Magnetite mixtures. Dependence of $|\mu|$ on concentration v .

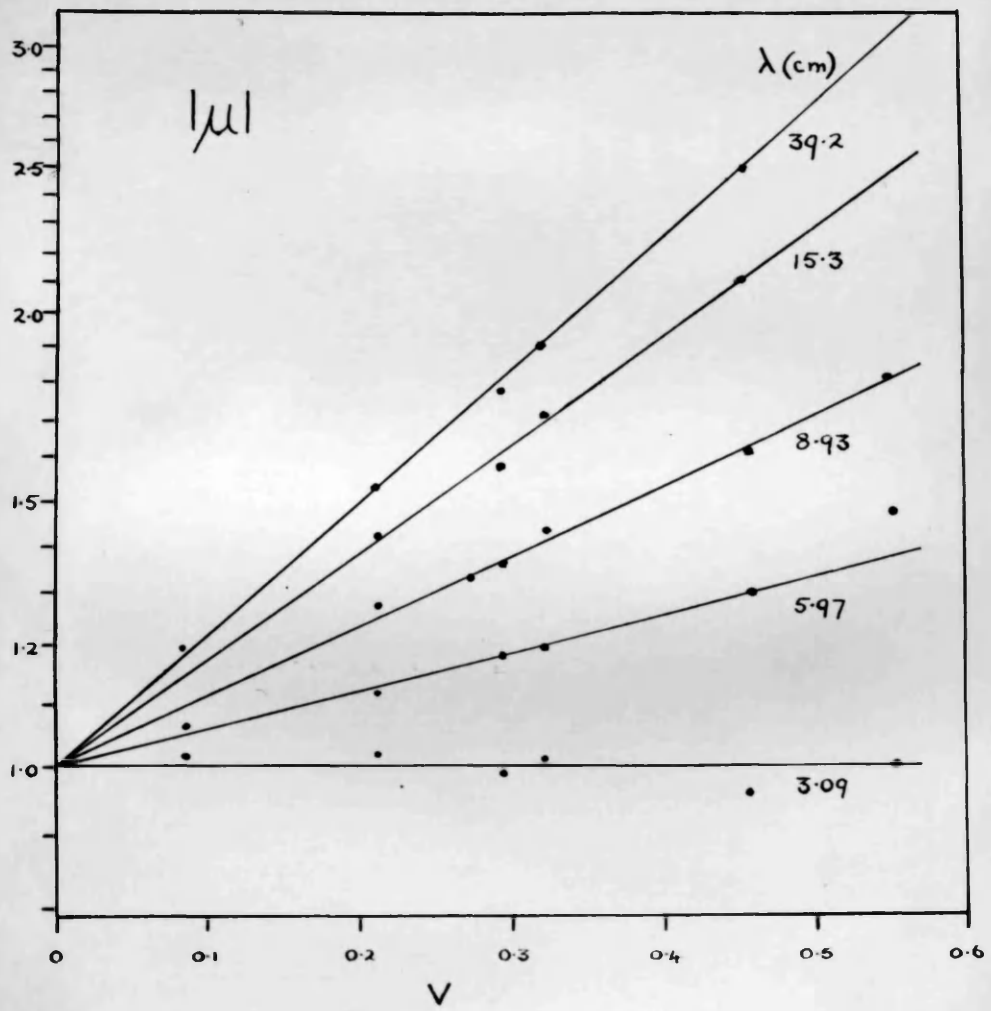

FIG. 13

Figure 14. Magnetite mixtures. Dependence of magnetic loss tangent on concentration.

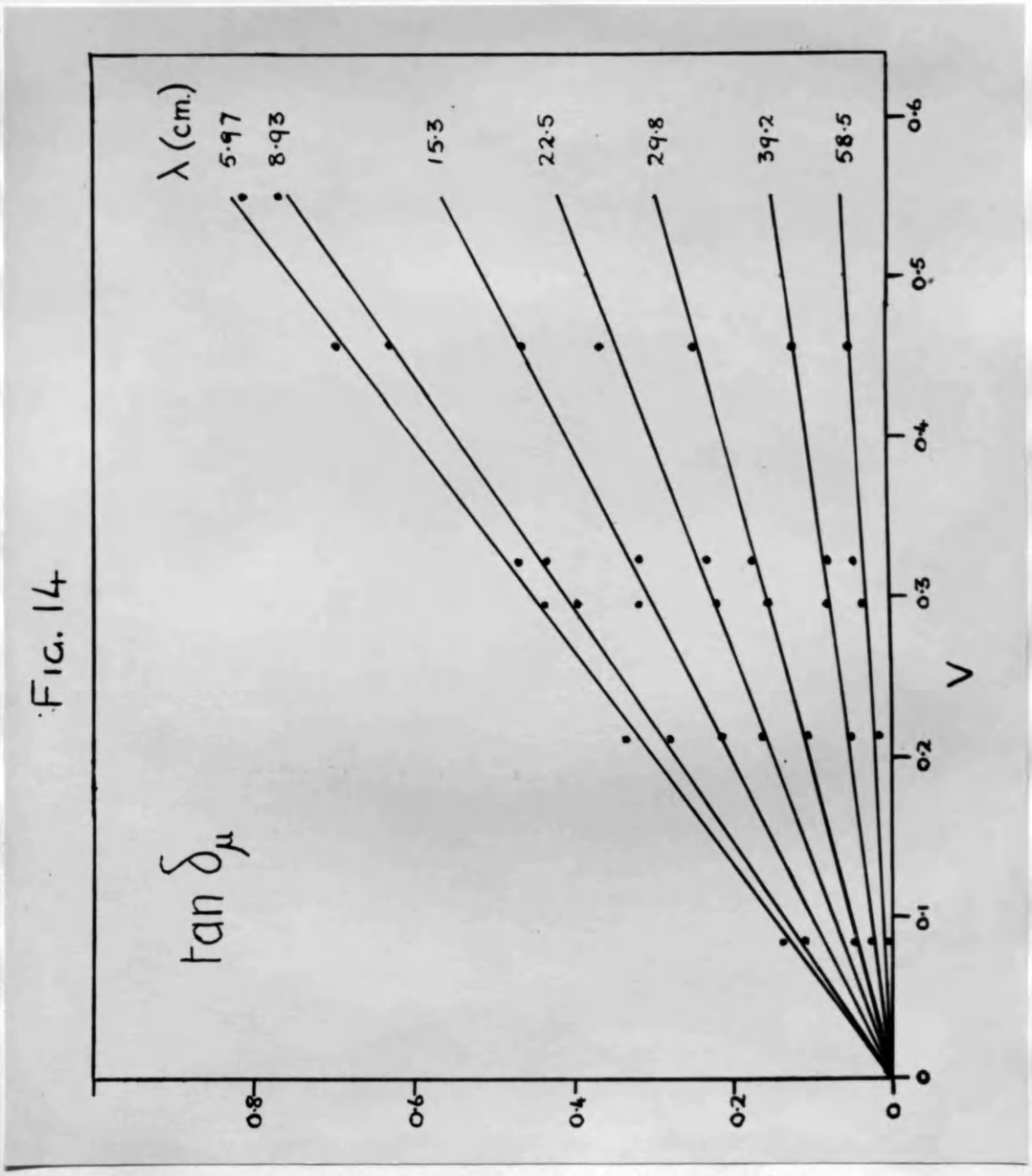

Figure 15. Magnetic dispersion and absorption of magnetite.

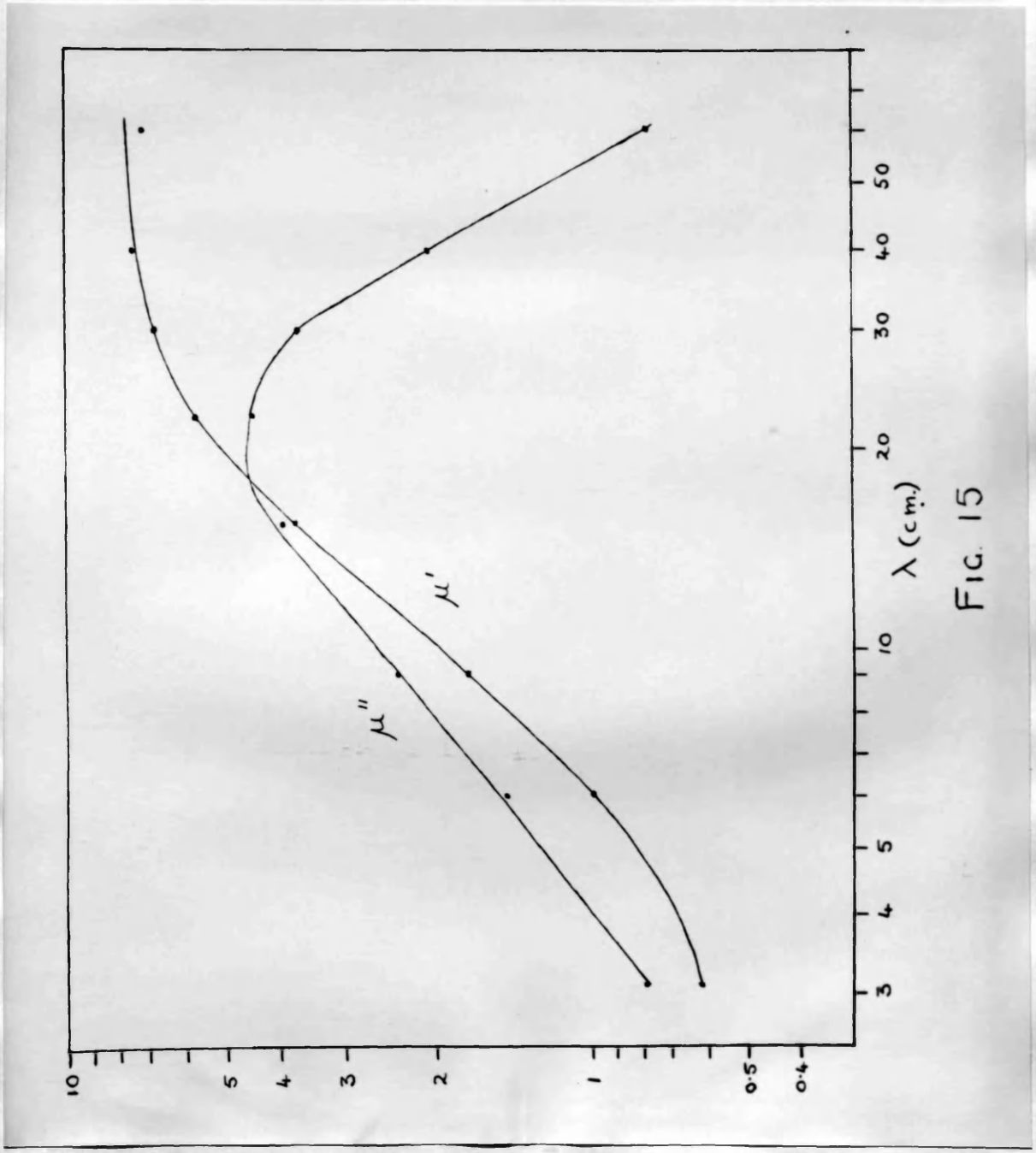

FIG. 15

Figure 16. Magnetic dispersion and absorption of manganese-zinc ferrite.

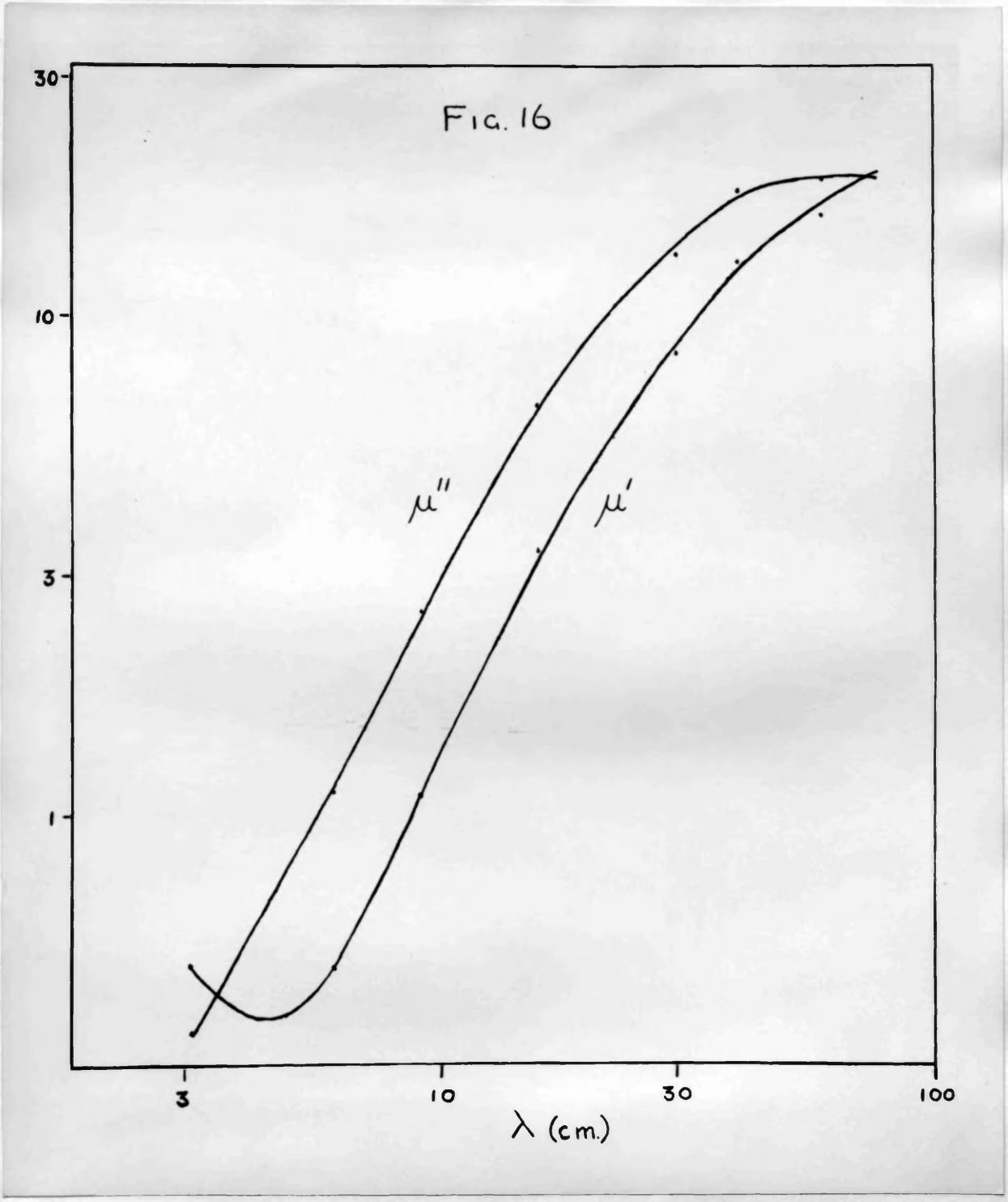

Figure 17. Magnetic dispersion and absorption of nickel-zinc ferrite.

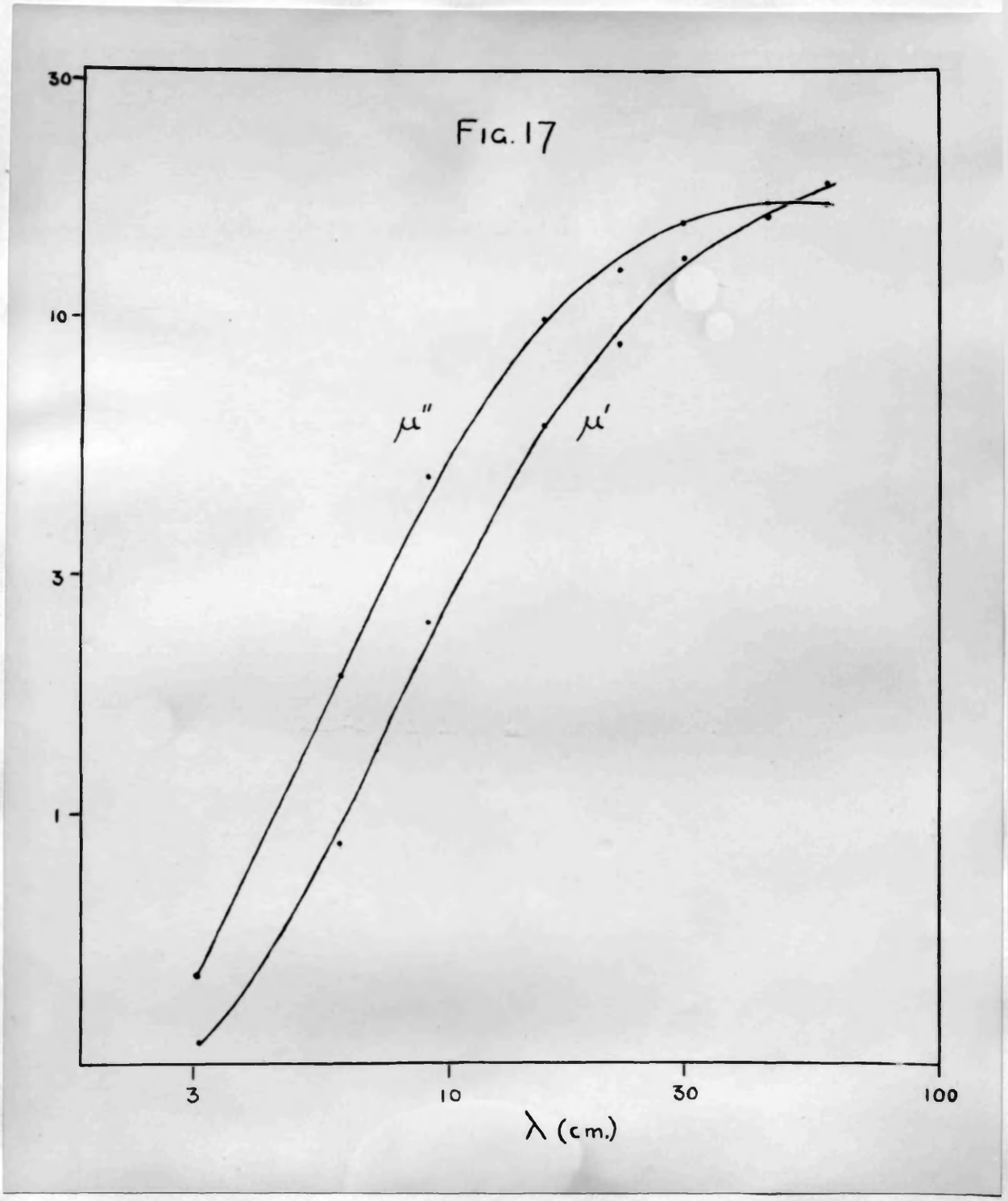

Figure 18. Magnetite. Comparison with single-resonance theory ($\mu_0 = 8$, $\nu_n = 5000$ Mc/s, $\nu' = 7500$ Mc/s).

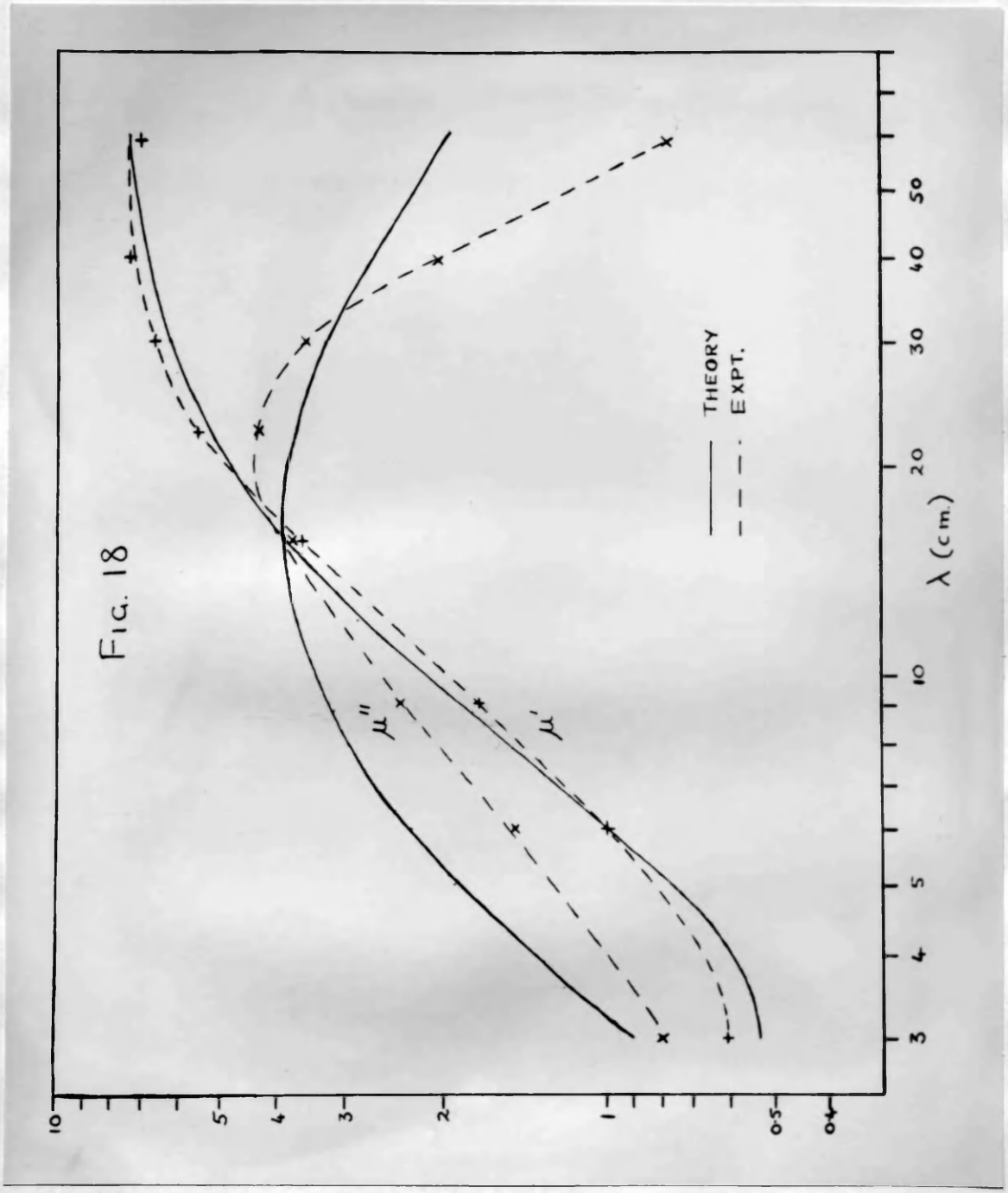

Figure 19. Rotational magnetisation process in a single domain.